Oncogenic RAS signaling is a tumor cell-intrinsic determinant of ferroptosis suppression via induction of the GCH1/BH4 axis

Jonathan K. M. Lim[1*], Frauke Stölting[1], Dennis Roth[2], Christian Ballmeyer[2], Sofya Tishina[3,4], Leonie Thewes[5], Simone Kalis[6], Samira Boussettaoui[6], Daniel Picard[1,7,8], Hai-Feng Zhang[9,10], Oksana Lewandowska[1,11], Tobias Reiff[11], Tal Levy[12,13], Barak Rotblat[12,13], Marc Remke[1,7,8], Poul H. Sorensen[9,10], Johannes Brägelmann[3,14,15], Filippo Beleggia[3,14,16], Carsten Berndt[5], Dirk Gründemann[6], Silvia von Karstedt[3,4,15], Guido Reifenberger[1,8], Georg Fluegen[2], Gabriel Leprivier[1*]

[1]Institute of Neuropathology, University Hospital Düsseldorf and Medical Faculty, Heinrich Heine University, Düsseldorf, Germany

[2]Department of General, Visceral and Pediatric Surgery, University Hospital Düsseldorf and Medical Faculty, Heinrich-Heine University, Düsseldorf, Germany

[3]University of Cologne, Faculty of Medicine and University Hospital Cologne, Department of Translational Genomics, Cologne, Germany

[4]University of Cologne, CECAD Cluster of Excellence, Cologne, Germany

[5]Department of Neurology, University Hospital Düsseldorf and Medical Faculty, Heinrich-Heine University Düsseldorf, Düsseldorf, Germany

[6]Department of Pharmacology, Faculty of Medicine and University Hospital Cologne, University of Cologne, Germany.

[7]Department of Pediatric Oncology, Hematology, and Clinical Immunology, University Hospital Düsseldorf and Medical Faculty, Heinrich Heine University, Düsseldorf, Germany

[8]Pediatric Oncology and Hematology, Children's Hospital, Saarland University, Homburg, Germany

[9]Department of Pathology and Laboratory Medicine, University of British Columbia, Vancouver, BC, Canada

[10]Department of Molecular Oncology, BC Cancer Agency, Vancouver, BC, Canada

[11]Institute of Genetics, Heinrich-Heine-University, Düsseldorf, Germany

[12]Department of Life Sciences, Faculty of Natural Sciences, Ben-Gurion University of the Negev, Beer-Sheva, Israel

[13]The National Institute for Biotechnology in the Negev, Ben-Gurion University of the Negev, Beer-Sheva, Israel

[14]University of Cologne, Faculty of Medicine and University Hospital Cologne, Mildred Scheel School of Oncology, Cologne, Germany

[15]University of Cologne, Faculty of Medicine and University Hospital Cologne, Center for Molecular Medicine, Cologne, Germany

[16]Department I of Internal Medicine, Faculty of Medicine and University Hospital Cologne, University of Cologne, Cologne, Germany

[*]Correspondence: jonathan.lim@med.uni-duesseldorf.de, gabriel.leprivier@med.uni-duesseldorf.de

Classification: Biological Sciences - Cell Biology

Keywords: RAS, oncogene, GCH1, ferroptosis

Abstract

Ferroptosis is an iron-dependent form of regulated cell death arising from excessive lipid peroxidation. The role of oncogenic RAS signaling in modulating the cellular response to ferroptosis is controversial. While seminal studies described that oncogenic RAS transformation drives a synthetic lethal vulnerability to archetypal ferroptosis inducers including erastin (eradicator of RAS and ST-expressing cells) and RSL3 (Ras selective lethal 3), more recent work suggest that oncogenic RAS signaling may confer ferroptosis resistance. Thus, the impact of oncogenic RAS expression on ferroptosis sensitivity is still poorly understood. Here, using orthogonal cellular systems across multiple classes of ferroptosis-inducing agents, as well as in silico therapeutic drug-response analyses, we provide unifying evidence that oncogenic RAS signaling suppresses ferroptosis. Integrated proteo- and transcriptomic analyses in oncogenic RAS-transformed cells further uncovered that RAS signaling upregulates the ferroptosis suppressor GTP cyclohydrolase I (GCH1) via transcriptional induction by the transcription factor ETS1 downstream of the RAS-MAPK signaling cascade. Targeted repression of Gch1 or of Gch1-controlled tetrahydrobiopterin (BH4) synthesis pathway is sufficient to sensitize RAS-mutant cell lines to ferroptosis in 2D and 3D cell models, as well as in tumor organoids and tumor xenografts, highlighting a mechanism through which RAS promotes resistance to ferroptosis induction. Furthermore, we found that *GCH1* expression is clinically relevant and correlates with RAS signaling activation in human cancers. Overall, this study redefines oncogenic RAS signaling to be a ferroptosis suppressor, and identifies GCH1 as a mediator of this effect and a potential clinical target for the sensitization of RAS-driven cancers to ferroptosis-inducing agents.

Significance Statement

Although it is commonly accepted that ferroptosis induction is a mutant RAS-selective lethality, accumulating evidence suggests that oncogenic RAS protects cells against this form of cell death. However, a systematic survey establishing the relationship between RAS and ferroptosis sensitivity is lacking, and the molecular mechanisms this entails are still poorly understood. Here, we report across RAS-mutant isoforms, in diverse cellular models, and using multiple ferroptosis-inducing compounds that oncogenic RAS consistently suppresses ferroptosis. Further, we show that oncogenic RAS-mediated ferroptosis suppression is attributed to the upregulation of GCH1 and its downstream metabolite, tetrahydrobiopterin. Our study delivers a shift towards a new paradigm in which oncogenic RAS confers ferroptosis resistance, and a potential clinical strategy to re-engage ferroptosis sensitivity in RAS-driven cancers.

Introduction

Ferroptosis is an iron-dependent, non-apoptotic form of cell death resulting from the excessive accumulation of lipid hydroperoxides. Cellular defenses against ferroptosis are mediated by the combined action of the cystine/glutamate antiporter xCT, which by importing the precursor cystine enables sufficient rates of glutathione (GSH) biosynthesis, a prerequisite for the enzymatic activity of glutathione peroxidase 4 (GPX4), the only enzyme detoxifying lipid hydroperoxides (1–4). Independent of the xCT-GPX4 axis, other major regulators of ferroptosis include ferroptosis suppressor protein 1 (FSP1), which mediates ubiquinol (CoQH2) recycling, and GTP cyclohydrolase 1 (GCH1), which mediates tetrahydrobiopterin (BH4) synthesis, both of which are lipophilic radical-trapping antioxidants with the propensity to reduce toxic lipid hydroperoxides (5–10). Ferroptosis has been implicated in cancer and is described to be modulated by tumor suppressors including p53 and BAP1, and oncogenes including MYCN and PI3K (11–14). Intriguingly, ferroptosis was discovered in synthetic lethal screens used to identify compounds that preferentially kill mutant RAS^{G12V} transformed cells but not normal isogenic counterparts – termed RAS-selective lethal (RSL) compounds, which include erastin (xCT inhibitor) and RSL3 (GPX4 inhibitor) (15–17). These initial studies and subsequent work consolidated a line of thought that oncogenic RAS sensitizes cells to ferroptosis (3, 18).

RAS is a small GTPase encoded by the *HRAS*, *KRAS*, and *NRAS* proto-oncogenes (19–21). Physiologically, RAS is responsible for transmitting growth factors signals from receptor tyrosine kinases through to the activation of the RAF-MEK-ERK and PI3K-AKT pathways, which promote proliferation and survival, respectively (20, 21). *RAS* genes are frequently mutated in human cancer, particularly in pancreatic, colorectal, and lung adenocarcinomas (21). Upon mutation, RAS acquires oncogenic properties that mediate tumor initiation and maintenance. Furthermore, oncogenic RAS confers resistance to apoptosis through multiple signaling cascades, rendering it difficult to target RAS-mutant tumors (22–24). Therefore, exploiting ferroptosis induction as a means to circumvent such resistance represents an attractive alternative approach to treating RAS-mutant cancers.

Nonetheless, the impact of oncogenic RAS on ferroptosis is still unclear. On the one hand, the first descriptions of ferroptosis are inextricably linked to its initial discovery as a RAS-selective lethality (15–17). Conversely, work by us and others demonstrate that oncogenic RAS enhances intracellular glutathione biosynthesis, which might be expected instead to confer protection against ferroptosis (25–28). Furthermore, we recently reported that oncogenic RAS induces FSP1 expression to mitigate RSL3-induced ferroptosis (29). Thus, a systematic investigation into the *bona fide* role of oncogenic RAS in modulating the response to ferroptosis is warranted.

Here, we examined the relationship between oncogenic RAS expression and ferroptosis sensitivity. We find that in orthogonal isogenic cell models, transformation with mutant KRAS or HRAS strongly suppresses ferroptosis induction across several classes of ferroptosis inducers (FINs), substantiating that oncogenic RAS signaling mediates the protection of cells, rather than their sensitization to ferroptosis induction. This was further supported by in silico analyses of therapeutic drug-response data showing correlations between activation of RAS signaling and ferroptosis resistance. Mechanistically, integrated transcriptome and proteomic profiling reveal that expression of the ferroptosis suppressor GTP cyclohydrolase I (GCH1), an enzyme controlling the tetrahydrobiopterin (BH4) synthesis pathway, is upregulated upon $KRAS^{G12V}$ transformation. Indeed, we provide evidence that *GCH1* transcription is under the regulation of the transcription factor ETS1 downstream of the RAS-driven RAF-MEK-ERK pathway. Functionally, we uncovered that GCH1 and BH4 synthesis contributes to oncogenic $KRAS^{G12V}$-mediated ferroptosis resistance in vitro and in vivo. This has clinical relevance as we report that *GCH1* expression is increased in RAS-mutant tumors. These results redefine the role of oncogenic RAS signaling to be a ferroptosis suppressor, and may potentially guide future strategies to maximize the clinical utility of ferroptosis-inducing compounds as next-generation therapeutic modalities against RAS-mutant tumors.

Results

Oncogenic RAS signaling activation confers resistance to ferroptosis

The role of oncogenic RAS in modulating cellular susceptibility to ferroptosis is still controversial. To provide unifying evidence as to the impact of oncogenic RAS on ferroptosis, we sought to interrogate the response of multiple isogenic cellular RAS systems to different classes of ferroptosis inducers (FINs). First, we found that mouse NIH 3T3 fibroblasts transformed with mutant $KRAS^{G12V}$ (NIH 3T3 $KRAS^{G12V}$) were completely resistant to the class I FINs erastin and sulfasalazine (SSZ), class II FINs ML162 and ML210, and class IV FIN FINO2, while non-transformed counterparts NIH 3T3 MSCV showed varying levels of cell death following a 16-hour treatment with each of these compounds (Fig. 1A and S1A). This is consistent with our previous findings that mouse embryonic fibroblasts display enhanced resistance to the class II FIN RSL3 following endogenous level expression of oncogenic KRAS (29). Co-treatment with the ferroptosis-selective antioxidant ferrostatin-1 (Fer-1) abolished cell death induced in non-transformed fibroblasts by the different FINs, confirming the induction of ferroptosis (Fig. 1A and Fig. S1A). Strikingly, NIH 3T3 $KRAS^{G12V}$ were completely resistant even when exposed to high concentrations of erastin (up to 20 μM), while non-transformed

145 cells were susceptible across a range of erastin treatment (Fig. S1A). Second, we confirmed
146 these initial observations using a derivative of a widely-utilized mutant RAS overexpression
147 system, namely human BJ fibroblasts immortalized with the catalytic subunit of human
148 telomerase (hTERT), SV40 large T and small T antigen (LT and ST respectively) and
149 transformed by ectopic expression of oncogenic HRAS^{G12V} (BJ-hTERT/LT/ST/HRAS^{G12V}, also
150 known as BJeLR cells) (2, 3, 30). This model previously led to the identification of RSL3 and
151 erastin as selective lethal agents against cells expressing both mutant RAS and small T
152 antigen (ST) (15–17). To determine the impact of mutant RAS in this model, but independently
153 of ST, we subjected BJ-hTERT/LT/HRAS^{G12V} and the corresponding isogenic BJ-hTERT/LT
154 control cells to FINs treatment. Interestingly, BJ-hTERT/LT/HRAS^{G12V} showed enhanced
155 resistance to RSL3, ML162, ML210 and erastin, as compared to BJ-TERT/LT (Fig. 1B), in
156 contrast to previous findings obtained with BJeLR compared to BJ-hTERT (15–17). While
157 these results further support that oncogenic RAS confers resistance against ferroptosis
158 induction, they also highlight the contribution of ST to ferroptosis sensitivity (15). In agreement
159 with increased resistance to multiple FINs and our previously reported data, BJ-
160 hTERT/LT/HRAS^{G12V} cells expressed higher levels of SLC7A11 and FSP1 than BJ-hTERT/LT
161 (Fig. S1, B and C) (26, 29). Third, to extend the validity of our findings in human cell lines, we
162 assessed the impact of KRAS depletion on susceptibility to ferroptosis, using shRNA-
163 mediated knockdown of KRAS in mutant KRAS^{G12V}-expressing human pancreatic
164 adenocarcinoma cell line CFPAC1. Notably, KRAS knockdown rendered CFPAC1 cells more
165 sensitive to RSL3-induced cell death, which was again rescued by Fer-1 (Fig. 1C and D).

166 Finally, to determine the generalizability of oncogenic RAS-mediated resistance to ferroptosis,
167 we leveraged cancer cell line drug sensitivity data from the Cancer Therapeutic Response
168 Portal v2 (CTRPv2), available from Broad Institute's DepMap portal (31, 32). We observed a
169 correlation across over 700 cancer cell lines between *KRAS* mutation and resistance (i.e.,
170 higher median area under the curve [AUC] values) to ML162 (Fig. 1E), while this was not
171 observed for RSL3, ML210, and erastin (Fig. S1, D to F). Given that the RAS pathway can be
172 active even in cancer cells harboring *KRAS wild-type* (*KRAS^{wt}*), due to various genetic events,
173 we analyzed RAS pathway activity in the same dataset using a validated transcriptional
174 signature of 84 genes (RAS84) optimized to capture RAS oncogenic activity (33). Remarkably,
175 we found that higher RAS pathway activation positively correlated with resistance to ML162,
176 RSL3, ML210, and erastin (Fig. 1, F to I). Taken together, these findings provide strong
177 evidence that oncogenic RAS signaling activation functionally protects cells from ferroptosis
178 and correlates with ferroptosis resistance across a large number of cancer cells.

179 **Oncogenic RAS signaling leads to upregulation of GCH1**

180 The fact that RAS pathway activation correlates with ferroptosis resistance across many
181 cancer entities suggests that it may be mediated by additional mechanisms besides FSP1 and
182 xCT upregulation. Therefore, we next sought to identify novel downstream mediators of
183 oncogenic RAS signaling that could protect cells against ferroptosis. To this end, we
184 performed RNA sequencing of NIH 3T3 KRAS^{G12V} and control cells and integrated this data
185 with our previous proteomics analysis performed on the same cell lines (34). These screens
186 identified 2022 transcripts and 448 proteins that were significantly altered following KRAS^{G12V}-
187 expression, among which were 193 overlapping transcripts/proteins (Fig. S2A). Consistent
188 with our prior investigations, transcriptome profiling identified *Slc7a11* and *Aifm2* (encoding
189 Fsp1), but not *Gpx4*, as upregulated by oncogenic RAS signaling (Fig. 2A). Notably, among
190 the 193 overlapping transcripts/proteins significantly altered in KRAS^{G12V}-expressing cells, the
191 gene encoding, *Gch1* represented the 5th most upregulated transcript and 10th most
192 upregulated protein (Fig. 2A and Table S1). GCH1 is the rate-limiting enzyme in BH4
193 biosynthesis, a radical-trapping antioxidant with potent activity against LP, and a suppressor
194 of ferroptosis (Fig. 2B) (7, 8). For this reason, we decided to focus on the regulation of *GCH1*
195 by oncogenic RAS. The upregulation of *Gch1* in NIH 3T3 KRAS^{G12V} versus control cells was
196 confirmed using qRT-PCR (Fig. 2C), as well as at the protein level using mass spectrometry-
197 based proteomics (Fig. 2D). In accordance with this, NIH 3T3 KRAS^{G12V} displayed elevated

levels of both BH4 as well as its oxidized form dihydrobiopterin (BH2) relative to control cells, suggesting that oncogenic activation of RAS signaling enhances de novo BH4 synthesis (Fig. 2E).

In agreement with our findings above, human BJ-hTERT/LT/HRAS^{G12V} cells showed a similar increase in *GCH1* expression relative to BJ-hTERT/LT isogenic counterparts (Fig. 2F). In human cancer cells harboring *KRAS* mutations, including CFPAC1 and non-small cell lung carcinoma cell line H460, shRNA-mediated knockdown of KRAS conversely led to decreases in *GCH1* expression (Fig. 2, G and H and Fig. S2B). Similarly, treatment of mutant KRAS^{G12C}-expressing pancreatic cancer cell line MIA PaCa-2 with the KRAS^{G12C} inhibitor AMG 510 decreased *GCH1* expression (Figure 2I).

Additionally, by analyzing expression data of IMR90 human fibroblasts we found elevated *GCH1* expression upon stable expression of HRAS^{G12V}, as compared to control pBabe, but not upon constitutively active AKT1 (Figure 2J) (35). This suggests that *GCH1* might be upregulated downstream of RAS-MAPK signaling but not PI3K-AKT signaling. To further ascertain this, we treated NIH 3T3 KRAS^{G12V} cells with the MEK inhibitor PD184352 or the AKT inhibitor MK-2206 and found that the former but not the latter led to decreased *Gch1* expression, further supporting that the regulation of *GCH1* downstream of oncogenic RAS is mediated by MAPK (RAF-MEK-ERK) signaling (Figure 2K). Moreover, MEK inhibition led to a sustained depletion of *Gch1* expression for up to 72 hours (Fig. S2C). Altogether, the data suggests that oncogenic RAS signaling leads to upregulation of *GCH1* expression in a MAPK-dependent manner.

GCH1 mediates oncogenic RAS-driven ferroptosis resistance

We next investigated the role of GCH1 in mediating ferroptosis suppression downstream of oncogenic RAS signaling. For these studies, we first employed ferroptosis sensitive non-transformed NIH 3T3 cells to determine whether supplementation with BH4, the end product of the biosynthesis pathway downstream of GCH1, could phenocopy ferroptosis resistance mediated by KRAS-mutant expression in these cells. Strikingly, cells supplemented with BH4 or BH2, showed near-complete insensitivity to erastin or FINO2, similar to NIH 3T3 KRAS^{G12V} cells (Fig. 3, A and B). While NIH 3T3 MSCV exhibited higher amounts of LP as NIH 3T3 KRAS^{G12V} cells when treated with erastin or FINO2, consistent with the ferroptosis-related phenotypes observed in these cells, the levels of LP were significantly reduced upon supplementation of NIH 3T3 MSCV with BH2 (Fig. 3, C and D). This was not the case with BH4 treatment (Fig. 3, C and D), suggesting a possible difference in the mechanism of ferroptosis protection between BH2 and BH4, or decreased BH4 efficiency since the oxidation of BH4 upon contact with culture medium may yield multiple oxidation products. Furthermore, BH4 or BH2 supplementation abrogated ferroptosis sensitivity of KRAS-knockdown CFPAC1 cells under RSL3 treatment (Fig. 3E), linking mutant KRAS-mediated ferroptosis resistance to the activity of the BH4 synthesis pathway. Finally, to ascertain of the contribution of GCH1 to KRAS^{G12V}-mediated resistance to ferroptosis, we knocked down *Gch1* expression in NIH 3T3 KRAS^{G12V} cells using CRISPR interference (CRISPRi). This was sufficient to restore the sensitivity of NIH 3T3 KRAS^{G12V} to ferroptosis induced by erastin or FINO2, which was reversed with BH4 or BH2 supplementation (Fig. 3F and G, Fig. S3A). Similarly, CRISPRi-mediated knockdown of *GCH1* expression in CFPAC1 cells sensitized them to RSL3-induced ferroptosis, while BH4 supplementation strongly reversed such effects, lending functional support to the observed positive correlation between *GCH1* expression and resistance to various FINs including RSL3 (Fig. 3H and Fig. S3B). Taken together, these findings suggest that oncogenic RAS signaling confers ferroptosis resistance by co-opting GCH1 function.

Targeting GCH1 or the BH4 synthesis pathway sensitizes oncogenic RAS-transformed cells to ferroptosis in vivo

Next, we sought to determine the contribution of GCH1 to oncogenic RAS-mediated tumorigenic potential or the ability of GCH1 inhibition to synergize with ferroptosis induction in

249 vivo. To this end, we first assessed the ability of NIH 3T3 KRAS^{G12V} cells to grow under
250 anchorage-independent conditions following CRISPRi-mediated *Gch1* knockdown using soft
251 agar colony formation assays. While knockdown of *Gch1* expression did not observably
252 decrease colony growth of KRAS-transformed cells under normal conditions, it resulted in
253 significantly decreased tumorigenic potential of these cells under conditions of ferroptosis
254 induction, suggesting that GCH1 inhibition may also synergize with ferroptosis induction in
255 vivo (Fig. 4A and Fig. S3C). Similarly, this effect was observed in KRAS-transformed cells
256 treated with AXSP0056 (GCH1i), a novel allosteric inhibitor against GCH1, or SPRi3, an
257 inhibitor against sepiapterin reductase (SPR), the enzyme mediating the final step of BH4
258 synthesis (Fig. 2B), under ferroptosis-induced conditions (Fig. 4B and C). In agreement,
259 GCH1i or SPRi3 treatment synergized with RSL3-mediated ferroptosis induction in reducing
260 the viability of pancreatic organoids derived from the LsL-KRAS^{G12D} transgenic mouse model
261 of pancreatic cancer (Fig. 4D, Fig. S3D) (36). Next, we investigated the effect of GCH1
262 inhibition on in vivo tumor growth using a chick chorio-allantoic membrane (CAM) assay, which
263 was previously shown to reliably recapitulate in vivo parameters of angiogenesis, tumor growth
264 and dissemination, as well as response to chemotherapeutics including FINs (37–39). In this
265 assay, NIH 3T3 KRAS^{G12V} cells were inoculated onto the upper CAM of fertilized chicken eggs,
266 then treated with FINO2, erastin, or vehicle every 2 days until the tumors were harvested and
267 measured 7 days following tumor cell inoculation. We observed that while *Gch1* knockdown
268 alone had no observable effects on tumor growth, combination with FINO2 treatment led to
269 significant tumor growth reduction (Fig. 4E, Fig. S3E). Interestingly, *Gch1* knockdown also
270 failed to synergize with erastin, consistent with previous studies showing its lack of potency or
271 metabolic stability in vivo (40). Altogether, our findings suggest that targeting BH4 synthesis
272 may be of therapeutic interest to sensitize RAS-mutant tumors to ferroptosis induction.

273 ***GCH1* expression is clinically relevant and correlates with oncogenic RAS activation in**
274 **human cancers**

275 It was previously reported that *GCH1* expression contributes to lung cancer, breast cancer,
276 and glioblastoma development and that its overexpression is linked to poor prognosis of
277 glioblastoma patients (41–43). Given the potential of GCH1 inhibition as a therapeutic strategy
278 for the sensitization of RAS driven tumors to ferroptosis induction, we now analyzed the clinical
279 relevance of *GCH1* expression in human cancers harboring KRAS mutation or constitutive
280 RAS signaling activation through analysis of The Cancer Genome Atlas (TCGA) datasets.
281 Notably, a pan-cancer analysis revealed that *GCH1* expression is higher in *KRAS-mutant*
282 (*KRAS^{mut}*) tumors than in *KRAS^{wt}* tumors (Fig. 5A). We then extended the same analysis of
283 *GCH1* expression to several tumor types of which a significant proportion of tumors are known
284 to harbour activating mutations in *KRAS*, namely pancreatic adenocarcinoma (PAAD), colon
285 adenocarcinoma (COAD) and lung adenocarcinoma (LUAD). Such analyses revealed that
286 *GCH1* is overexpressed in PAAD, COAD, and LUAD relative to corresponding non-tumor
287 tissue (Fig. 5, B, C, and D). Further, *GCH1* overexpression was confirmed in two orthogonal
288 PAAD datasets (Fig. S4A and B) (44, 45). Consistent with the above-findings, we observed a
289 positive correlation between *GCH1* levels and RAS signaling activation (based on RAS84
290 signature) in COAD, but also in several other human cancers including rectal adenocarcinoma
291 (READ), uterine carcinosarcoma (UCS), skin cutaneous melanoma (SKCM), low-grade glioma
292 (LGG), and GBM (Fig. 5E-J). Of note, *GCH1* expression was recently reported to be elevated
293 in glioblastoma but the mechanisms by which this occurs remains unclear (41). Together with
294 previous reports that genetic alterations in components of the RAS-MAPK cascade are
295 frequently observed in glioblastoma, our evidence suggests that *GCH1* overexpression is
296 associated with oncogenic RAS signaling activation in this tumor type (46). In agreement,
297 over-representation analysis of genes positively co-expressed with *GCH1* in glioblastoma
298 exhibited significant enrichment of genes known to be upregulated upon KRAS activation (Fig.
299 5K). Moreover, *Gch1* levels are higher in tumors derived from a genetically engineered mouse
300 model of high-grade glioma, constituted from *Nf1*-deletion (which promotes RAS pathway
301 activation), as compared to matched normal tissue (Fig. 5L), but this was not observed in a *c-*

302 *Myc*-driven mouse model of liver carcinoma (Fig. S4C) (47). Together, our findings reveal the
303 clinical relevance of *GCH1* regulation by the oncogenic RAS pathway in human cancers.

304 **Transcriptional upregulation of *GCH1* by oncogenic RAS signaling is mediated by ETS1**

305 We next sought to determine the mechanism by which oncogenic RAS signaling regulates
306 *GCH1* expression. To this end, we conducted gene set enrichment analysis (GSEA) of genes
307 displaying positive co-expression with *Gch1* from the above RNA sequencing data of NIH 3T3
308 $KRAS^{G12V}$ and control cells. Notably, genes having at least one binding site for the transcription
309 factor Ets-1 showed significant enrichment, and this gene set was among the top five
310 transcription factor target gene sets showing enrichment (Fig. 6A, Fig. S5A). Given the fact
311 that ETS1 is a known substrate of ERK downstream of the RAS-MAPK signaling pathway, we
312 postulated that the regulation of *GCH1* by oncogenic RAS is mediated by ETS1, which to our
313 knowledge has not been reported (Fig. 6B). In support of this, siRNA-mediated knockdown of
314 *Ets-1* expression in NIH 3T3 $KRAS^{G12V}$ cells significantly decreased *Gch1* expression (Fig.
315 6C). Similarly, knockdown of *ETS1* expression in H460 cells using two distinct siRNAs led to
316 a decrease in *GCH1* expression (Fig. 6D). Next, to ascertain whether ETS1 controls the
317 induction of *GCH1*, we performed dual-luciferase reporter assays in HEK293T cells using a
318 reporter construct consisting of a transcriptionally active region (TAR) of *GCH1* directly
319 upstream of *Firefly luciferase*. Sequence analysis of this region revealed the presence of three
320 ETS1 binding sites, based on the consensus 5'-GGAA/T-3' (Fig. 6E). While ectopic ETS1
321 expression was sufficient to activate the TAR of *GCH1* in a dose-dependent manner,
322 mutations in each of three putative ETS1 binding sites within this region abrogated this effect,
323 with concurrent mutations in all three sites having the strongest effect (Fig. 6, F and G). In
324 support of this, chromatin immunoprecipitation (ChIP)-qRT-PCR in NIH 3T3 $KRAS^{G12V}$ cells
325 and ChIP-sequencing analysis of publicly-available UCSC Encode data provided strong
326 evidence that endogenous ETS1 occupies the human and mouse TAR region of *GCH1* (Fig.
327 6, H and I). Consistent with our functional analyses above, pan-cancer data from the Clinical
328 Proteomic Tumor Analysis Consortium (CPTAC) indicate that *GCH1* expression levels are
329 positively correlated with ETS1 protein expression (Fig. 6J), whereas publicly-available PAAD,
330 COAD, and LUAD datasets similarly show a positive correlation between *GCH1* and *ETS1*
331 mRNA expression (Fig. 6, K to M) (45, 48, 49). Together, these data support that *GCH1* is
332 transcriptionally upregulated by the MEK-ERK-ETS1 pathway downstream of oncogenic RAS.

333 **Discussion**

334 There is a growing interest in the potential of inducing ferroptosis in tumor cells as an
335 anticancer strategy. However, ferroptosis sensitivity varies substantially among cancer cells
336 due to distinct tissue lineages, mutation status of oncogenes or tumor suppressor genes, as
337 well as the acquisition of drug-tolerant or differentiated cell states (3, 11, 50–52). Thus,
338 understanding the mechanisms that contribute to lipid peroxidation and ferroptosis will aid the
339 development of effective approaches to overcome ferroptosis resistance. In this study, we
340 demonstrate that oncogenic activation of RAS signaling, one of the most mutated pathways
341 in cancer, is a major tumor cell-intrinsic determinant of ferroptosis resistance. Notably,
342 ferroptosis originally emerged as an alternative form of necrosis induced by erastin and RSL3,
343 identified from synthetic lethal compound screens for their selective cytotoxicity towards
344 engineered mutant HRAS-overexpressing cells known as BJeLR cells (15–17). Following
345 these seminal findings, the identification of novel classes of FINs have often been
346 accompanied by validation in the BJeLR model, over time substantiating a paradigm that
347 oncogenic RAS-transformed cells are ostensibly sensitive to ferroptosis inducers, even though
348 the association between KRAS mutational status and ferroptosis sensitivity could never be
349 confirmed in comprehensive human cancer cell line screens (3, 53). On the contrary, our
350 findings here, together with our previous study suggest rather that oncogenic RAS signaling
351 renders cells resistant to ferroptosis, as demonstrated using multiple functional models (29).
352 One of the models used here, BJ-hTERT/LT/$HRAS^{V12}$ cells, are similar to BJeLR but allowed
353 us to interrogate the effect of mutant RAS independently of ST, which was initially used as an

354 additional transforming factor. Indeed, in the absence of ST, mutant HRAS^{V12} expression led
355 to a paradoxical resistance to FINs suggesting that the presence of ST may confound the
356 contribution of RAS signaling in modulating the sensitivity of cells to ferroptosis. Notably, one
357 of the mechanisms by which ST promotes malignant transformation is by negatively regulating
358 the protein phosphatase 2A (PP2A) family (30). Thus, the mechanisms by which ST or PP2A
359 possibly modulate ferroptosis response warrant further investigation.

360 It was previously suggested that the expression level of mutant RAS, whether expressed from
361 an endogenous locus or ectopically overexpressed, will have differential effects on ferroptosis
362 sensitivity of the cell, depending ultimately on the net outcome of how cellular processes
363 related to ferroptosis, including metabolism, redox and iron homeostasis, are balanced (27,
364 29, 54). This could plausibly explain why oncogenic RAS sensitizes cells to ferroptosis in some
365 contexts, while in others protect cells from ferroptosis. However, our previous findings in
366 endogenous KRAS cellular models and current findings in ectopic cellular KRAS and HRAS
367 models, all demonstrate protection from FINs upon KRAS/HRAS-mutant expression. An
368 independent study similarly observed that rhabdomyosarcoma cells were protected against
369 ferroptosis upon ectopic expression of various oncogenic RAS isoforms (55). In support of
370 this, our survey of a large array of cancer cell lines (from the CCLE database) also revealed a
371 significant association between oncogenic RAS signaling activation and ferroptosis
372 resistance. Altogether, our evidence from various contexts are in accordance with a role of
373 oncogenic RAS signaling as a ferroptosis suppressor, and highlights that the accepted view
374 of ferroptosis as a synthetic lethal vulnerability of RAS-driven tumors needs to be revisited.

375 Another major finding of our work is that oncogenic activation of the RAS signaling pathway
376 induces *GCH1* transcription to promote ferroptosis suppression. GCH1 is the rate-limiting
377 enzyme in de novo synthesis of cellular BH4, converting GTP to dihydroneopterin phosphate
378 (NH2TP), which is further processed to 6-pyruvoyltetrahydropterin (6-PTP) via 6-
379 pyruvoyltetrahydropterin synthase (PTS), and finally producing BH4 via SPR (Fig. 2B) (56). In
380 turn, BH4 is an essential cofactor for a number of enzymes including nitric oxide synthases
381 (NOSs) and tyrosine hydroxylase, critical for the synthesis of nitric oxide (NO) and dopamine
382 respectively. More recently, BH4 itself was described to be a potent antioxidant with the ability
383 to trap lipid radicals and prevent the propagation of lipid peroxidation chain reaction, as well
384 as to selectively prevent oxidative degradation of polyunsaturated fatty acyl chain-containing
385 phospholipids that drive ferroptosis execution (7, 8). Consistently, we found that *GCH1*-
386 depletion re-sensitized KRAS-mutant cells to ferroptosis induction, while BH4
387 supplementation potently rescued this effect. In our cellular models, a direct radical-trapping
388 effect of BH4 is likely, but an indirect effect of BH4 from its cofactor role cannot be completely
389 ruled out. Intriguingly, BH4 reduction leads to uncoupling of NOSs, resulting in superoxide
390 generation, which can promote ferroptosis. Conversely, NO, even though considered a radical
391 species, paradoxically has been described to suppress ferroptosis by terminating LP
392 propagation (57). Further, evidence suggest that GCH1 overexpression leads to an
393 accumulation of the antioxidant CoQH2, since BH4 is also a cofactor for phenylalanine to
394 tyrosine conversion, which can generate 4-OH-benzoate, a precursor for CoQH2 synthesis
395 (7). It is therefore conceivable that BH4 generation downstream of oncogenic RAS signaling
396 could also protect cells against ferroptosis via NOS- or CoQH2-dependent mechanisms. Of
397 note, although the enhancement of GCH1-mediated BH4 synthesis is sufficient to suppress
398 ferroptosis, oxidized BH4 (BH2) can also be regenerated via the function of dihydrofolate
399 reductase (DHFR) (8). Thus, whether DHFR serves a compensatory role for BH4 maintenance
400 under GCH1-depleted conditions, and whether simultaneously targeting BH4 synthesis and
401 DHFR using pharmacological inhibitors may be a viable therapeutic strategy against RAS-
402 driven cancers, is likely to be a subject of future interest.

403 Our results are broadly consistent with the recent findings that EGFR and KRAS signaling
404 promotes *Gch1* expression in a genetically-engineered murine lung cancer model (42).
405 However, our study did not find any evidence in vitro or in vivo supporting that genetic ablation
406 of GCH1 alone leads to decreased tumorigenic potential. Instead, our results suggest a direct

role for GCH1 in the RAS-mediated protective response against ferroptosis, which has never been addressed. One possibility to explain why GCH1 inhibition alone did not show any effects is the absence of a fully functional immune system in our in vivo model. Another possibility is that the previously reported negative impact of GCH1 depletion on tumor growth is a result of exacerbating a pre-existing oxidizing environmental condition in vivo, since lung cancer may have high basal levels of lipid peroxidation due to extensive lipid remodeling and exposure to high O_2 levels (58). Mechanistically, we additionally demonstrate that the transcriptional upregulation of GCH1 downstream of RAS activation is mediated by MAPK signaling and its associated transcription factor ETS1.

Our study adds to a growing body of literature substantiating a role for GCH1 and BH4 metabolism in tumor development (41, 43, 59). In this context, while targeting GCH1 alone could be a viable therapeutic strategy to target cancers including difficult-to-treat RAS-mutant tumors, our findings suggest that combining inhibitors of the BH4 pathway with FINs, such as FINO2, may represent a more effective therapeutic approach. Alternatively, combining RAS pathway inhibitors with FINs may prove to be an attractive therapeutic strategy since we and others have shown that repressing RAS signaling may sensitize cells to FINs, and particularly in light of now well-documented resistance to RAS inhibitors (60, 61).

In summary, this study uncovers that oncogenic RAS signaling transcriptionally regulates the GCH1-BH4 axis to mediate ferroptosis resistance. Along with our previous work, we postulate that oncogenic RAS signaling may induce an extensive transcriptional program promoting the upregulation of three major arms of ferroptosis defense which also includes the xCT-glutathione axis and the FSP1-CoQH2 axis (26, 29). Collectively, our findings offer 1) a renewed perspective for the role of oncogenic RAS as a predictor of ferroptosis resistance, which holds significant future ramifications for the clinical application of FINs as a cancer therapy 2) the mechanism by which this occurs, and 3) the translational potential of inhibiting GCH1/BH4 as a novel strategy for the sensitization of refractory and recurrent RAS-mutant tumors to ferroptosis.

Materials and Methods

Cell culture

NIH 3T3 cells expressing mutant $KRAS^{G12V}$ and control MSCV were generated and cultured as previously described (26). BJ cells expressing human telomerase (hTERT), SV40 large T (LT) and mutant $HRAS^{G12V}$ (hTERT/LT/$HRAS^{G12V}$) and control hTERT/LT were a kind gift from William C. Hahn (Dana-Farber Cancer Institute, Boston, U. S. A). H460 cells were a kind gift from Julian Downward (Francis Crick Institute, London, UK). MIA PaCa-2 cells were a kind gift from Barbara Grüner (German Cancer Consortium DKTK, Essen, Germany). HEK293T and CFPAC1 cells were purchased from American Type Culture Collection (Rockville, MD). Unless otherwise specified, all cell lines were maintained in DMEM (Gibco) supplemented with 10% fetal calf serum (FCS; Sigma Aldrich). All cells were kept at 37 °C with 5% CO2 and tested for mycoplasma at regular intervals.

Murine pancreatic tumor organoids treatment

Pancreatic tumor organoids were generated as previously described (29). For GCH1i, organoids were seeded at 100 cells/well and allowed to grow for one week following which GCH1i (500 μM), RSL3 (1 μM), or Vehicle treatment were added alone, or in combination for an additional 48 hours. For SPRi3, organoids were seeded at 100 cells/well with SPRi3 (50 μM) or Vehicle treatment and allowed to grow for one week following which RSL3 (1 μM) treatments were added for an additional 48 hours. Organoid sizes were imaged and quantified using the BZ-H4M/Measurement Application Software (Keyence).

Full Materials and Methods available in Supplemental information

Acknowledgements

Research in the lab of G.L. was funded by the Deutsche Forschungsgemeinschaft (grant no. LE 3751/2-1), the German Cancer Aid (grants no. 70112624, 70115129 and 70116491), the Dr. Rolf M. Schwiete Stiftung (grant no. 2020-018) and the Research Commission of the Medical Faculty, Heinrich Heine University Düsseldorf (grants no. 2016-056, 2020-044 and 2022-25). J.K.M.L was supported by the Deutsche Forschungsgemeinschaft (Walter Benjamin Fellowship no. LI3844/1-1), the Dr. Rolf M. Schwiete Stiftung (grant no. 2023-029) and the Research Commission of the Medical Faculty, Heinrich Heine University Düsseldorf (grant no. 2022-12). Research in the lab of G.F. was funded by the Deutsche Forschungsgemeinschaft (grant no. 422215274). Research in the lab of S.v.K was funded by: a collaborative research center grant on cell death (CRC1403, project ID 414786233), predictability in evolution (CRC1310, project ID 325931972), small cell lung cancer (CRC1399, project ID 413326622), B-cell lymphomas (CRC1530, project ID 455784452), through a priority program on ferroptosis (SPP2306, project ID 461704389) all funded by the Deutsche Forschungsgemeinschaft, an eMed consortium grant by the BMBF (InCa-01ZX1901A), via CANTAR which is funded through the program " Netzwerke 2021", an initiative of the Ministry of Culture and Science of the State of Northrhine Westphalia, Germany and a project grant (A06) funded by the center for molecular medicine cologne (CMMC). Research in the lab of F.B. was funded by the Deutsche Forschungsgemeinschaft (SFB1399 grant no. 41332662), the German Cancer Aid (grants no. 70113041, 70116707 and Mildred Scheel Nachwuchszentrum grant no. 70113307). J.B. was funded by: a collaborative research center grant on small cell lung cancer (CRC1399 grant no. 413326622) by the Deutsche Forschungsgemeinschaft, via CANTAR which is funded through the program " Netzwerke 2021", an initiative of the Ministry of Culture and Science of the State of Northrhine Westphalia, Germany, a career advancement grant by the Center for Molecular Medicine Cologne (CMMC, CAP18) and the Mildred Scheel Nachwuchszentrum (grant no. 70113307). C.B. was funded by the Deutsche Forschungsgemeinschaft via GRK2578 (project ID 417677437).

Author contributions

Conceptualization, J.K.M.L. and G.L.; Methodology, J.K.M.L., F.S., D.R., C.B., T.L., L.T., S.K., S.B., D.P., S.T., H.Z., O.L., J.B., F.B., D.G., G.F.; Resources, T.R., M.R., C.B., S.v.K., G.R., B.R., D.G., G.F.; Writing – Original Draft, J.K.M.L and G.L.; Writing – Review & Editing, J.K.M.L., F.S., S.T., H.Z., T.R., F.B., S.v.K., G.R., B.R., and G.L.; Visualization, J.K.M.L. and G.L.; Supervision, J.K.M.L and G.L.; Funding Acquisition, J.K.M.L., B.R., G.R. and G.L.

Competing interests

J.B. has received a research grant by Bayer AG outside of the presented work. The other authors declare no potential competing interests.

References

1. S. J. Dixon, *et al.*, Ferroptosis: an iron-dependent form of nonapoptotic cell death. *Cell* **149**, 1060–1072 (2012).
2. S. J. Dixon, *et al.*, Pharmacological inhibition of cystine-glutamate exchange induces endoplasmic reticulum stress and ferroptosis. *Elife* **3**, e02523 (2014).
3. W. S. Yang, *et al.*, Regulation of ferroptotic cancer cell death by GPX4. *Cell* **156**, 317–331 (2014).
4. J. P. Friedmann Angeli, *et al.*, Inactivation of the ferroptosis regulator Gpx4 triggers acute renal failure in mice. *Nat Cell Biol* **16**, 1180–1191 (2014).
5. S. Doll, *et al.*, FSP1 is a glutathione-independent ferroptosis suppressor. *Nature* **575**, 693–698 (2019).
6. K. Bersuker, *et al.*, The CoQ oxidoreductase FSP1 acts parallel to GPX4 to inhibit ferroptosis. *Nature* **575**, 688–692 (2019).
7. V. A. N. Kraft, *et al.*, GTP Cyclohydrolase 1/Tetrahydrobiopterin Counteract Ferroptosis through Lipid Remodeling. *ACS Cent Sci* **6**, 41–53 (2020).
8. M. Soula, *et al.*, Metabolic determinants of cancer cell sensitivity to canonical ferroptosis inducers. *Nat Chem Biol* **16**, 1351–1360 (2020).

508 9. H.-F. Zhang, R. I. Klein Geltink, S. J. Parker, P. H. Sorensen, Transsulfuration, minor
509 player or crucial for cysteine homeostasis in cancer. *Trends Cell Biol* **32**, 800–814
510 (2022).
511 10. C. Berndt, *et al.*, Ferroptosis in health and disease. *Redox Biol* **75**, 103211 (2024).
512 11. L. Jiang, *et al.*, Ferroptosis as a p53-mediated activity during tumour suppression.
513 *Nature* **520**, 57–62 (2015).
514 12. Y. Zhang, *et al.*, BAP1 links metabolic regulation of ferroptosis to tumour suppression.
515 *Nat Cell Biol* **20**, 1181–1192 (2018).
516 13. H. Alborzinia, *et al.*, MYCN mediates cysteine addiction and sensitizes neuroblastoma to
517 ferroptosis. *Nat Cancer* **3**, 471–485 (2022).
518 14. J. Yi, J. Zhu, J. Wu, C. B. Thompson, X. Jiang, Oncogenic activation of PI3K-AKT-mTOR
519 signaling suppresses ferroptosis via SREBP-mediated lipogenesis. *Proc Natl Acad Sci U*
520 *S A* **117**, 31189–31197 (2020).
521 15. S. Dolma, S. L. Lessnick, W. C. Hahn, B. R. Stockwell, Identification of genotype-
522 selective antitumor agents using synthetic lethal chemical screening in engineered
523 human tumor cells. *Cancer Cell* **3**, 285–296 (2003).
524 16. N. Yagoda, *et al.*, RAS-RAF-MEK-dependent oxidative cell death involving voltage-
525 dependent anion channels. *Nature* **447**, 864–868 (2007).
526 17. W. S. Yang, B. R. Stockwell, Synthetic lethal screening identifies compounds activating
527 iron-dependent, nonapoptotic cell death in oncogenic-RAS-harboring cancer cells. *Chem*
528 *Biol* **15**, 234–245 (2008).
529 18. I. Poursaitidis, *et al.*, Oncogene-Selective Sensitivity to Synchronous Cell Death
530 following Modulation of the Amino Acid Nutrient Cystine. *Cell Rep* **18**, 2547–2556
531 (2017).
532 19. J. L. Bos, ras oncogenes in human cancer: a review. *Cancer Res* **49**, 4682–4689 (1989).
533 20. J. Downward, Targeting RAS signalling pathways in cancer therapy. *Nat Rev Cancer* **3**,
534 11–22 (2003).
535 21. Y. Pylayeva-Gupta, E. Grabocka, D. Bar-Sagi, RAS oncogenes: weaving a tumorigenic
536 web. *Nat Rev Cancer* **11**, 761–774 (2011).
537 22. A. D. Cox, C. J. Der, The dark side of Ras: regulation of apoptosis. *Oncogene* **22**, 8999–
538 9006 (2003).
539 23. S. von Karstedt, *et al.*, Cancer cell-autonomous TRAIL-R signaling promotes KRAS-
540 driven cancer progression, invasion, and metastasis. *Cancer Cell* **27**, 561–573 (2015).
541 24. F. J. H. Hoogwater, *et al.*, Oncogenic K-Ras turns death receptors into metastasis-
542 promoting receptors in human and mouse colorectal cancer cells. *Gastroenterology* **138**,
543 2357–2367 (2010).
544 25. E. M. Kerr, E. Gaude, F. K. Turrell, C. Frezza, C. P. Martins, Mutant Kras copy number
545 defines metabolic reprogramming and therapeutic susceptibilities. *Nature* **531**, 110–113
546 (2016).
547 26. J. K. M. Lim, *et al.*, Cystine/glutamate antiporter xCT (SLC7A11) facilitates oncogenic
548 RAS transformation by preserving intracellular redox balance. *Proc Natl Acad Sci U S A*
549 **116**, 9433–9442 (2019).
550 27. J. K. M. Lim, G. Leprivier, The impact of oncogenic RAS on redox balance and
551 implications for cancer development. *Cell Death Dis* **10**, 955 (2019).
552 28. J. K. M. Lim, G. Leprivier, P. H. Sorensen, RAS-driven oncogenesis is supported by
553 downstream antioxidant programs. *Mol Cell Oncol* **7**, 1654814 (2020).
554 29. F. Müller, *et al.*, Elevated FSP1 protects KRAS-mutated cells from ferroptosis during
555 tumor initiation. *Cell Death Differ* **30**, 442–456 (2023).
556 30. W. C. Hahn, *et al.*, Enumeration of the simian virus 40 early region elements necessary
557 for human cell transformation. *Mol Cell Biol* **22**, 2111–2123 (2002).
558 31. A. Tsherniak, *et al.*, Defining a Cancer Dependency Map. *Cell* **170**, 564-576.e16 (2017).
559 32. F. M. Behan, *et al.*, Prioritization of cancer therapeutic targets using CRISPR-Cas9
560 screens. *Nature* **568**, 511–516 (2019).
561 33. P. East, *et al.*, RAS oncogenic activity predicts response to chemotherapy and outcome
562 in lung adenocarcinoma. *Nat Commun* **13**, 5632 (2022).

563 34. H.-F. Zhang, *et al.*, Proteomic Screens for Suppressors of Anoikis Identify IL1RAP as a
564 Promising Surface Target in Ewing Sarcoma. *Cancer Discov* **11**, 2884–2903 (2021).
565 35. A. L. Kennedy, *et al.*, Activation of the PIK3CA/AKT pathway suppresses senescence
566 induced by an activated RAS oncogene to promote tumorigenesis. *Mol Cell* **42**, 36–49
567 (2011).
568 36. S. R. Hingorani, *et al.*, Preinvasive and invasive ductal pancreatic cancer and its early
569 detection in the mouse. *Cancer Cell* **4**, 437–450 (2003).
570 37. D. Fischer, *et al.*, The CAM Model-Q&A with Experts. *Cancers (Basel)* **15**, 191 (2022).
571 38. B. Hassannia, *et al.*, Nano-targeted induction of dual ferroptotic mechanisms eradicates
572 high-risk neuroblastoma. *J Clin Invest* **128**, 3341–3355 (2018).
573 39. L. B. Pontel, *et al.*, Acute lymphoblastic leukemia necessitates GSH-dependent
574 ferroptosis defenses to overcome FSP1-epigenetic silencing. *Redox Biol* **55**, 102408
575 (2022).
576 40. Y. Zhang, *et al.*, Imidazole Ketone Erastin Induces Ferroptosis and Slows Tumor Growth
577 in a Mouse Lymphoma Model. *Cell Chem Biol* **26**, 623-633.e9 (2019).
578 41. A. N. Tran, *et al.*, Reactive species balance via GTP cyclohydrolase I regulates
579 glioblastoma growth and tumor initiating cell maintenance. *Neuro Oncol* **20**, 1055–1067
580 (2018).
581 42. S. J. F. Cronin, *et al.*, Phenotypic drug screen uncovers the metabolic GCH1/BH4
582 pathway as key regulator of EGFR/KRAS-mediated neuropathic pain and lung cancer.
583 *Sci Transl Med* **14**, eabj1531 (2022).
584 43. Z. Wang, *et al.*, GTP Cyclohydrolase Drives Breast Cancer Development and Promotes
585 EMT in an Enzyme-Independent Manner. *Cancer Res* **83**, 3400–3413 (2023).
586 44. L. Badea, V. Herlea, S. O. Dima, T. Dumitrascu, I. Popescu, Combined gene expression
587 analysis of whole-tissue and microdissected pancreatic ductal adenocarcinoma identifies
588 genes specifically overexpressed in tumor epithelia. *Hepatogastroenterology* **55**, 2016–
589 2027 (2008).
590 45. R. Janky, *et al.*, Prognostic relevance of molecular subtypes and master regulators in
591 pancreatic ductal adenocarcinoma. *BMC Cancer* **16**, 632 (2016).
592 46. M. Ceccarelli, *et al.*, Molecular Profiling Reveals Biologically Discrete Subsets and
593 Pathways of Progression in Diffuse Glioma. *Cell* **164**, 550–563 (2016).
594 47. A. Méndez-Lucas, *et al.*, Identifying strategies to target the metabolic flexibility of
595 tumours. *Nat Metab* **2**, 335–350 (2020).
596 48. S. Cherradi, P. Martineau, C. Gongora, M. Del Rio, Claudin gene expression profiles and
597 clinical value in colorectal tumors classified according to their molecular subtype. *Cancer*
598 *Manag Res* **11**, 1337–1348 (2019).
599 49. A. L. Tarca, *et al.*, Strengths and limitations of microarray-based phenotype prediction:
600 lessons learned from the IMPROVER Diagnostic Signature Challenge. *Bioinformatics*
601 **29**, 2892–2899 (2013).
602 50. M. J. Hangauer, *et al.*, Drug-tolerant persister cancer cells are vulnerable to GPX4
603 inhibition. *Nature* **551**, 247–250 (2017).
604 51. V. S. Viswanathan, *et al.*, Dependency of a therapy-resistant state of cancer cells on a
605 lipid peroxidase pathway. *Nature* **547**, 453–457 (2017).
606 52. J. Tsoi, *et al.*, Multi-stage Differentiation Defines Melanoma Subtypes with Differential
607 Vulnerability to Drug-Induced Iron-Dependent Oxidative Stress. *Cancer Cell* **33**, 890-
608 904.e5 (2018).
609 53. R. P. Abrams, W. L. Carroll, K. A. Woerpel, Five-Membered Ring Peroxide Selectively
610 Initiates Ferroptosis in Cancer Cells. *ACS Chem Biol* **11**, 1305–1312 (2016).
611 54. G. M. DeNicola, *et al.*, Oncogene-induced Nrf2 transcription promotes ROS
612 detoxification and tumorigenesis. *Nature* **475**, 106–109 (2011).
613 55. C. Schott, U. Graab, N. Cuvelier, H. Hahn, S. Fulda, Oncogenic RAS Mutants Confer
614 Resistance of RMS13 Rhabdomyosarcoma Cells to Oxidative Stress-Induced
615 Ferroptotic Cell Death. *Front Oncol* **5**, 131 (2015).
616 56. B. Thöny, G. Auerbach, N. Blau, Tetrahydrobiopterin biosynthesis, regeneration and
617 functions. *Biochem J* **347 Pt 1**, 1–16 (2000).

57. T. Homma, *et al.*, Nitric oxide protects against ferroptosis by aborting the lipid peroxidation chain reaction. *Nitric Oxide* **115**, 34–43 (2021).
58. C. Bartolacci, *et al.*, Targeting de novo lipogenesis and the Lands cycle induces ferroptosis in KRAS-mutant lung cancer. *Nat Commun* **13**, 4327 (2022).
59. J. Liu, *et al.*, QDPR deficiency drives immune suppression in pancreatic cancer. *Cell Metab* **36**, 984-999.e8 (2024).
60. V. Bhatt, *et al.*, Inhibition of autophagy and MEK promotes ferroptosis in Lkb1-deficient Kras-driven lung tumors. *Cell Death Dis* **14**, 61 (2023).
61. M. M. Awad, *et al.*, Acquired Resistance to KRASG12C Inhibition in Cancer. *N Engl J Med* **384**, 2382–2393 (2021).
62. H. Thorvaldsdóttir, J. T. Robinson, J. P. Mesirov, Integrative Genomics Viewer (IGV): high-performance genomics data visualization and exploration. *Brief Bioinform* **14**, 178–192 (2013).

Fig. 1. Oncogenic activation of RAS signaling suppresses ferroptosis. (A) Cell death quantification of NIH 3T3 cells expressing mutant $KRAS^{G12V}$ or control MSCV upon treatment with ML162 (2 μM), ML210 (10 μM), FINO2 (20 μM), sulfasalazine (SSZ; 0.7 mM) or vehicle for 24 h in the presence or absence of ferrostatin-1 (Fer-1; 5 μM), analyzed by propidium iodide (PI) staining and flow cytometry. (B) Cell death quantification of BJ cells expressing human telomerase (hTERT), SV40 large T (LT) and mutant $HRAS^{G12V}$ (hTERT/LT/$HRAS^{G12V}$) or control hTERT/LT upon treatment with RSL3 (1 μM), ML162 (0.5 μM), ML210 (1 μM), erastin (ERA; 5 μM) or vehicle for 24 h in the presence or absence of Fer-1 (5 μM), analyzed as in (A). (C) Cell death quantification of shKRAS knockdown and scrambled (scr) control CFPAC1 cells upon treatment with indicated concentrations of RSL3 for 24 h in the presence or absence of Fer-1 (5 μM), analyzed as in (A) and (B). (D) Relative *KRAS* mRNA expression in shKRAS knockdown and scr control CFPAC1 cells analyzed by qRT-PCR. (E) Correlation between *KRAS* mutation status and sensitivity to ML162 in cancer cells. *wt, wild-type. mut, mutant*. (F, G, H, and I) Correlation between *RAS* signature score and sensitivity to ML162, RSL3, ML210, and erastin in cancer cells. RAS^{low} and RAS^{high} cells are divided according to median AUC. (E-I) Data are obtained from the Cancer Therapeutic Response Portal v2 (CTRPv2) database, accessed via the DepMap portal. Higher AUC values indicate increased resistance to compound treatment. Data represent mean ± SD of three independent experiments. Unpaired, two-tailed *t test*; $^{*}P < 0.05$, $^{**}P < 0.01$, $^{***}P < 0.001$. ns, not significant.

Fig. 2. Oncogenic RAS signaling transcriptionally upregulates GCH1. (A) Volcano plots comparing transcriptomic (RNA sequencing) and proteomic profiles of NIH 3T3 cells expressing mutant $KRAS^{G12V}$ versus control MSCV. (B) Schematic depicting GCH1-mediated tetrahydrobiopterin (BH4) biosynthesis. (C) Relative *Gch1* mRNA expression in NIH 3T3 cells expressing mutant $KRAS^{G12V}$ and control MSCV analyzed by qRT-PCR. (D) Relative Gch1 peptide level in NIH 3T3 cells expressing mutant $KRAS^{G12V}$ and control MSCV analyzed by mass spectrometry. (E) Relative quantification of BH4 and BH2 levels in NIH 3T3 cells expressing mutant $KRAS^{G12V}$ and control MSCV analyzed by mass spectrometry. Each data point represents one sample measured across three independent experiments. (F) Relative *GCH1* mRNA expression in BJ cells expressing human telomerase (hTERT), SV40 large T (LT) and mutant $HRAS^{G12V}$ (hTERT/LT/$HRAS^{G12V}$) or control hTERT/LT analyzed by qRT-PCR. (G) Relative *GCH1* mRNA expression in shKRAS knockdown and scrambled (scr) control CFPAC1 cells analyzed by qRT-PCR. (H) Relative *GCH1* mRNA expression in shKRAS knockdown and scr control H460 cells analyzed by qRT-PCR. (I) Relative *GCH1* mRNA expression analyzed by qRT-PCR and phosphorylated ERK (p-ERK) levels analyzed by Western Blot, in MIA PaCa-2 cells upon treatment with AMG510 (10 μM) or vehicle for the indicated times. (J) Relative *GCH1* mRNA expression in IMR90 cells expressing myristoylated AKT1 (myrAKT1), mutant $HRAS^{G12V}$, or control pBabe, analyzed by microarray. Data are obtained from GSE45276, accessed via the R2 platform (http://r2.amc.nl) (35). (K) Relative *Gch1* mRNA expression analyzed by qRT-PCR, and expression of indicated proteins

671 analyzed by Western Blot in NIH 3T3 cells expressing mutant KRAS^{G12V} (NIH 3T3 KRAS^{G12V})
672 upon treatment with MEK inhibitor PD184352 (MEKi; 10 μM), AKT inhibitor MK2206 (AKTi ;
673 10 μM) or vehicle for the indicated times. Data represent mean ± SD of three independent
674 experiments. Unpaired, two-tailed *t test*; **P* < 0.05, ***P* < 0.01, ****P* < 0.001. ns, not significant.

675 **Fig. 3.** GCH1 mediates oncogenic RAS-driven ferroptosis suppression in 2D models. (A) Cell
676 death quantification of NIH 3T3 cells expressing mutant KRAS^{G12V} or control MSCV upon
677 treatment with indicated concentrations of erastin (Era) or vehicle for 24 h in the presence or
678 absence of dihydrobiopterin (BH2; 50 μM), tetrahydrobiopterin (BH4; 50 μM), or ferrostatin-1
679 (Fer-1; 5 μM), analyzed by propidium iodide (PI) staining and flow cytometry. (B) Cell death
680 quantification of NIH 3T3 cells expressing mutant KRAS^{G12V} or control MSCV upon treatment
681 with indicated concentrations of FINO2 or vehicle for 24 h in the presence or absence of BH2
682 (50 μM), BH4 (50 μM), or Fer-1 (5 μM), analyzed as in (A). (C) Lipid peroxidation quantification
683 of NIH 3T3 cells expressing mutant KRAS^{G12V} or control MSCV upon treatment with indicated
684 concentrations of Era or vehicle for 6 h in the presence or absence of BH2 (50 μM), BH4 (50
685 μM), or Fer-1 (5 μM), analyzed by C11-BODIPY(581/591) staining and flow cytometry. (D)
686 Lipid peroxidation quantification of NIH 3T3 cells expressing mutant KRAS^{G12V} or control
687 MSCV upon treatment with indicated concentrations of FINO2 or vehicle for 6 h in the
688 presence or absence of dihydrobiopterin BH2 (50 μM), BH4 (50 μM), or Fer-1 (5 μM), analyzed
689 as in (C). (E) Cell death quantification of shKRAS knockdown CFPAC1 cells upon treatment
690 with RSL3 (5 μM) for 24 h in the presence or absence of BH2 (50 μM) or BH4 (50 μM),
691 analyzed as in (A) and (B). (F) Relative *Gch1* mRNA expression in CRISPR interference
692 (CRISPRi)-mediated Gch1 knockdown (sgGch1-1 and sgGch1-2) and EGFP knockdown
693 (sgEGFP) control NIH 3T3 cells expressing mutant KRAS^{G12V} (NIH 3T3 KRAS^{G12V}), analyzed
694 by qRT-PCR. (G) Cell death quantification of sgGch1-1, sgGch1-2, and sgEGFP NIH 3T3
695 KRAS^{G12V} cells upon treatment with indicated concentrations of Era or vehicle for 24 h in the
696 presence or absence of BH2 (50 μM) or BH4 (50 μM), or Fer-1 (5 μM), analyzed as in (A) and
697 (B). (H) Cell death quantification of sgGCH1-1, sgGCH1-2, and sgEGFP CFPAC1 cells upon
698 treatment with indicated concentrations of RSL3 or vehicle for 24 h in the presence or absence
699 of BH4 (50 μM), or Fer-1 (5 μM), analyzed as in (A) (B) and (G). Data represent mean ± SD
700 of three independent experiments. Unpaired, one-tailed *t test*; **P* < 0.05, ***P* < 0.01, ****P* <
701 0.001. ns, not significant.

702 **Fig. 4.** GCH1 mediates oncogenic RAS-driven ferroptosis suppression in 3D models and in
703 vivo. (A) Colony formation of CRISPR interference (CRISPRi)-mediated Gch1 knockdown
704 (sgGch1-1 and sgGch1-2) and control (sgEGFP) NIH 3T3 cells expressing mutant KRAS^{G12V}
705 (NIH 3T3 KRAS^{G12V}) grown in soft agar for 21 days and treated with the indicated
706 concentrations of RSL3. Colonies were imaged and quantified using ImageJ, and normalized
707 to control. (B) Colony formation of NIH 3T3 KRAS^{G12V} cells grown in soft agar for 21 days and
708 treated with GCH1i (200 μM) or RSL3 (0.5 μM) alone or in combination. Colonies were imaged
709 and quantified using ImageJ. (C) Colony formation of NIH 3T3 KRAS^{G12V} cells grown in soft
710 agar for 21 days and treated with SPRi3 (20 μM) or RSL3 (0.5 μM), alone or in combination.
711 Colonies were imaged and quantified as in (A). (D) Pancreatic organoids were treated with
712 GCH1i (500 μM) or RSL3 (1 μM) alone or in combination for 48 hours. Organoids were imaged
713 and quantified using the BZ-H4M/Measurement Application Software (Keyence). (E) sgGch1-
714 1 and sgEGFP NIH 3T3 KRAS^{G12V} cells were inoculated onto the upper chorioallantoic
715 membrane (CAM) of post-fertilized (d7) specific-pathogen-free chicken (SPF) eggs and
716 treated with 50 μM FINO2 according to the indicated scheme following which tumors were
717 harvested and measured 7 days following inoculation. Data represent mean ± SD of three
718 independent experiments. Unpaired, one-tailed *t test*; **P* < 0.05, ***P* < 0.01, ****P* < 0.001. ns,
719 not significant.

720 **Fig. 5.** GCH1 expression is clinically relevant and correlates with oncogenic RAS activation in
721 human cancers. (A) Pan-cancer analysis of *GCH1* expression in tumor samples stratified
722 according to *KRAS* mutation status. *wt, wild-type. mut, mutant*. Data are obtained from The
723 Cancer Genome Atlas (TCGA), analyzed using the cBioPortal platform. (B, C, and D) *GCH1*

724 expression in tumor samples of pancreatic adenocarcinoma (PAAD), colon adenocarcinoma
725 (COAD), and lung adenocarcinoma (LUAD) from TCGA, in comparison to corresponding non-
726 tumor tissue from TCGA and/or Genotype-Tissue Expression (GTEx) database. Data are
727 analyzed using the UCSC Xena portal. (E, F, G, H, I, and J) Correlation of *GCH1* expression
728 and *RAS* signature score in tumor samples of COAD, rectal adenocarcinoma (READ), uterine
729 carcinosarcoma (UCS), skin cutaneous melanoma (SKCM), low-grade glioma (LGG), and
730 glioblastoma (GBM). Data are obtained from TCGA, accessed via the DepMap portal.
731 Correlations were quantified using Spearman's rank correlation coefficient. (K) Over-
732 representation analysis for Human Molecular Signatures Database (MSigDB) Hallmark gene
733 sets of genes positively co-expressed with *GCH1* in tumor samples of GBM from TCGA,
734 analyzed using the R2 platform. (L) *Gch1* expression in tumor samples from a mouse model
735 of high-grade glioma with *p53fl/fl;Nf1fl/fl* driven by Ascl1 Cre-ERTM, in comparison to non-tumor
736 tissue, obtained from GSE57036, accessed via the R2 platform. Data represent mean ± SD
737 of three independent experiments. Unpaired, two-tailed *t test*; $*P < 0.05$, $**P < 0.01$, $***P <$
738 0.001. ns, not significant.

739 **Fig. 6.** Transcriptional upregulation of GCH1 by oncogenic RAS signaling is mediated by
740 ETS1. (A) Gene set enrichment analysis (GSEA) of NIH 3T3 cells expressing mutant
741 $KRAS^{G12V}$ (NIH 3T3 $KRAS^{G12V}$) versus control MSCV showing enrichment for ETS1-regulated
742 genes. (B) Schematic depicting regulation of ETS1 downstream of RAS-MAPK signaling
743 pathway. (C) Relative *Gch1* mRNA expression analyzed by qRT-PCR and Ets-1 levels
744 analyzed by Western Blot in siRNA-mediated Ets-1 knockdown (siEts-1) and scrambled
745 (siScr) control NIH 3T3 $KRAS^{G12V}$ cells. (D) Relative *GCH1* mRNA expression analyzed by
746 qRT-PCR and ETS1 levels analyzed by Western Blot in si-ETS1 knockdown (siETS1-1 and
747 siETS1-2) and siScr control H460 cells. (E) Schematic depicting the transcriptionally active
748 region (TAR) of *GCH1* and ETS1 binding sites. (F) Activity measurements of a reporter
749 construct consisting of the TAR of *GCH1* directly upstream of *Firefly luciferase* (FLuc; *GCH1-*
750 *Luc*), normalized to control *Renilla luciferase* (RLuc), upon co-expression with the indicated
751 amounts of *ETS1*-expressing plasmid in HEK293T cells, and ETS1 expression levels
752 analyzed by Western Blot. *A. U., Arbitrary units*. (G) Activity measurements of *GCH1-Luc* or
753 *GCH1-Luc* with mutations in individual *ETS1* binding sites ($GCH1^{mut}$-*Luc*-1, 2, or 3) or all ETS1
754 binding sites ($GCH1^{mut}$-*Luc*-all) normalized to RLuc, upon co-expression with 400 ng of *ETS1*-
755 expressing plasmid in HEK293T cells, and ETS1 expression levels analyzed by Western Blot.
756 (H) ChIP-qPCR analysis showing occupancy of Ets-1 at the *Gch1* locus in NIH 3T3 $KRAS^{G12V}$
757 cells. (I) ChIP-sequencing data showing ETS1, H3K4me3, and H3K27ac occupancy profiles
758 at the *GCH1* locus, in HepG2 cells. Data are obtained from UCSC Encode database, analyzed
759 using Integrative Genomics Viewer (IGV) (62). (J) Correlation between *GCH1* expression and
760 ETS1 protein levels across multiple tumor entities from the Clinical Proteomic Tumor Analysis
761 Consortium (CPTAC) and TCGA, analyzed using the cBioPortal platform. (K, L, and M)
762 Correlation of *GCH1* expression and *ETS1* expression in tumor samples of PAAD, COAD, and
763 lung adenocarcinoma (LUAD) obtained from GSE62165, GSE72970, and GSE43580
764 respectively, accessed via the R2 platform (45, 48, 49). Correlations were quantified using
765 Spearman's rank correlation coefficient. Data represent mean ± SD of three independent
766 experiments. Unpaired, two-tailed *t test*; $*P < 0.05$, $**P < 0.01$, $***P < 0.001$. ns, not significant.

767 **Fig. S1.** (A) Cell death quantification of NIH 3T3 cells expressing mutant $KRAS^{G12V}$ or control
768 MSCV upon treatment with the indicated concentrations of erastin (Era) or vehicle for 24 h in
769 the presence or absence of ferrostatin-1 (Fer-1; 5 μM), analyzed by propidium iodide (PI)
770 staining and flow cytometry. (B and C) Relative *GCH1* and *xCT* mRNA expression in BJ cells
771 expressing human telomerase (hTERT), SV40 large T (LT) and mutant $HRAS^{G12V}$
772 (hTERT/LT/$HRAS^{G12V}$) or control hTERT/LT analyzed by qRT-PCR. Data represent the
773 mean ± SEM. (D, E, and F) Correlation between *KRAS* mutation status and sensitivity to RSL3,
774 ML210, and erastin in cancer cells. *wt, wild-type. mut, mutant*. Data are obtained from the
775 CTRP database, accessed via the DepMap portal. Data represent mean ± SD of three

independent experiments. Unpaired, two-tailed *t test*; *$P < 0.05$, **$P < 0.01$, ***$P < 0.001$. ns, not significant.

Fig. S2. (A) *left,* Venn diagram depicting significantly altered transcripts and proteins (fold change > 2 or < -2; $p < 0.05$) in NIH 3T3 cells expressing mutant $KRAS^{G12V}$ relative to control MSCV based on RNA sequencing and proteomic profiling. *right*, Heatmap showing concordance in transcript and protein levels of 193 overlapping transcripts/proteins significantly altered in $KRAS^{G12V}$-expressing cells. (B) Relative *KRAS* mRNA expression in shKRAS knockdown and scrambled (scr) control H460 cells analyzed by qRT-PCR. (C) Relative *Gch1* mRNA expression in NIH 3T3 cells expressing mutant $KRAS^{G12V}$ (NIH 3T3 $KRAS^{G12V}$) upon treatment with MEK inhibitor PD184352 (MEKi; 10 μM) or vehicle for the indicated times, analyzed by qRT-PCR. Data represent mean ± SD of three independent experiments. Unpaired, two-tailed *t test*; *$P < 0.05$, **$P < 0.01$, ***$P < 0.001$. ns, not significant.

Fig. S3. (A) Cell death quantification of sgGch1-1, sgGch1-2, and sgEGFP NIH 3T3 $KRAS^{G12V}$ cells upon treatment with indicated concentrations of FINO2 or vehicle for 24 h in the presence or absence of dihydrobiopterin (BH2; 50 μM) or tetrahydrobiopterin (BH4; 50 μM), or ferrostatin-1 (Fer-1; 5 μM), analyzed by propidium iodide (PI) staining and flow cytometry. (B) Ranking of correlation scores between GCH1 expression and sensitivity to CTRP compounds (median AUC). Data are obtained from the Cancer Therapeutic Response Portal v2 (CTRPv2) database, accessed via the DepMap portal. (C) Colony formation of CRISPR interference (CRISPRi)-mediated Gch1 knockdown (sgGch1-1 and sgGch1-2) and control (sgEGFP) NIH 3T3 cells expressing mutant $KRAS^{G12V}$ (NIH 3T3 $KRAS^{G12V}$) grown in soft agar for 21 days. Colonies were imaged and quantified using ImageJ, and normalized to control. (D) Pancreatic organoids were seeded with or without SPRi3 (50 μM) and allowed to grow for one week following which RSL3 (1 μM) treatments were added for 48 hours. Organoids were imaged and quantified using the BZ-H4M/Measurement Application Software (Keyence). (E) sgGch1-1 and sgEGFP NIH 3T3 $KRAS^{G12V}$ cells were inoculated onto the upper chorioallantoic membrane (CAM) of post-fertilized (d7) specific-pathogen-free chicken (SPF) eggs and treated with 10 μM erastin (Era) or Vehicle according to the scheme as shown in Fig. 4E following which tumors were harvested and measured 7 days following inoculation. Data represent mean ± SD of three independent experiments. Unpaired, one-tailed *t test*; *$P < 0.05$, **$P < 0.01$, ***$P < 0.001$. ns, not significant.

Fig. S4. (A and B) *GCH1* expression in tumor samples of PAAD in comparison to non-tumor tissue, obtained from GSE15471 and GSE62165, accessed via the R2 platform (44, 45) (C) *Gch1* expression in tumor samples from a mouse model of liver cancer driven by human c-MYC overexpression, in comparison to non-tumor tissue, obtained from GSE129013, accessed via the NCBI Gene Expression Omnibus (GEO) platform (47). Data represent mean ± SD of three independent experiments. Unpaired, two-tailed *t test*; *$P < 0.05$, **$P < 0.01$, ***$P < 0.001$. ns, not significant.

Fig. S5. (A) Gene set enrichment analysis (GSEA) of NIH 3T3 cells expressing mutant $KRAS^{G12V}$ (NIH 3T3 $KRAS^{G12V}$) versus control MSCV showing enrichment for target genes regulated by indicated transcription factors. (B) Correlation of *GCH1* expression and *ETS1* expression in tumor samples of pancreatic adenocarcinoma (PAAD) obtained from GSE15471 accessed via the R2 platform (44). Correlations were quantified using Spearman's rank correlation coefficient. Data represent mean ± SD of three independent experiments. Unpaired, two-tailed *t test*; *$P < 0.05$, **$P < 0.01$, ***$P < 0.001$. ns, not significant.

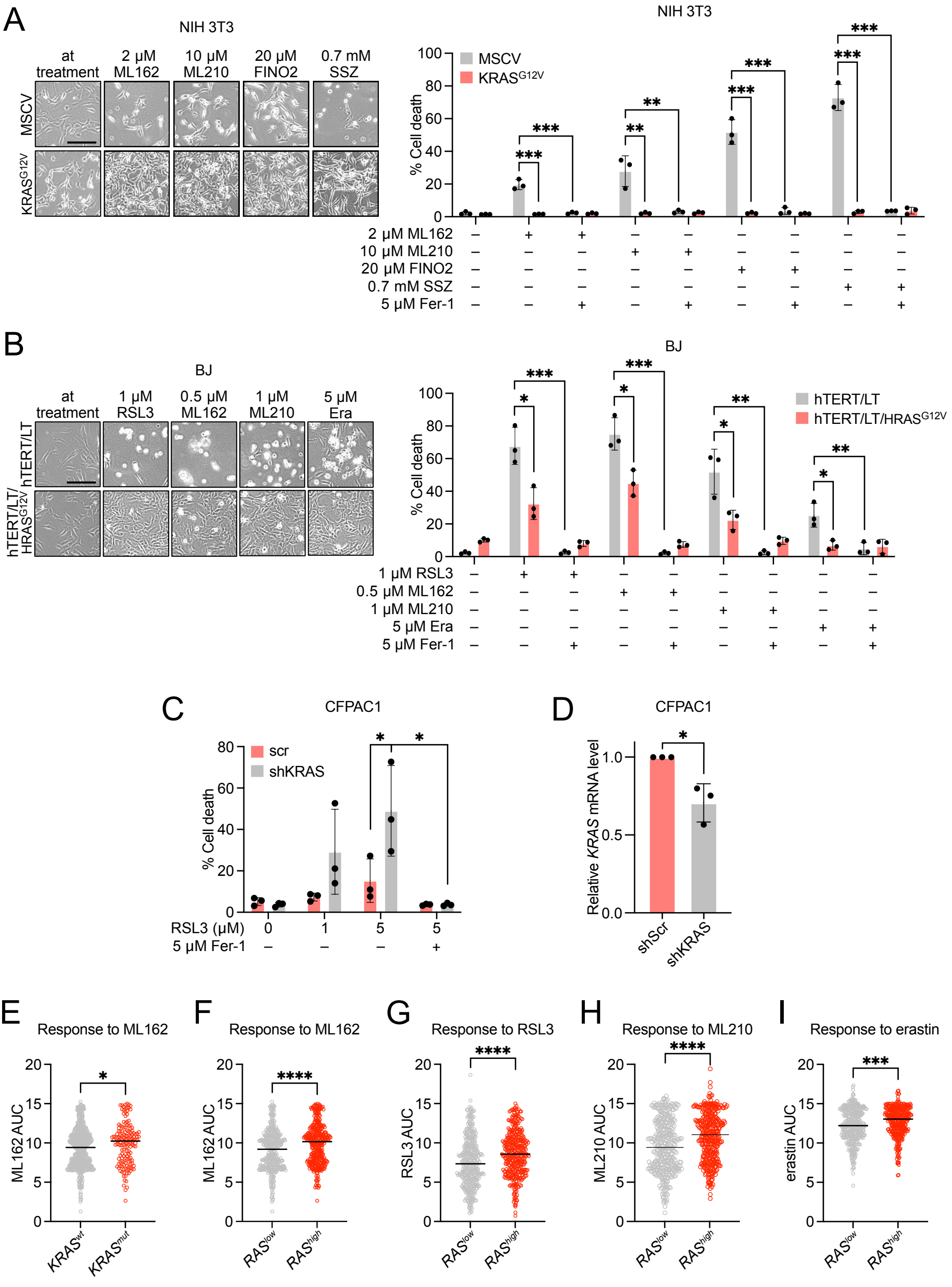
A
NIH 3T3
at treatment
2 μM ML162
10 μM ML210
20 μM FINO2
0.7 mM SSZ
MSCV
KRASG12V
MSCV
KRASG12V
% Cell death
2 μM ML162
10 μM ML210
20 μM FINO2
0.7 mM SSZ
5 μM Fer-1
B
BJ
at treatment
1 μM RSL3
0.5 μM ML162
1 μM ML210
5 μM Era
hTERT/LT
hTERT/LT/HRASG12V
hTERT/LT
hTERT/LT/HRASG12V
% Cell death
1 μM RSL3
0.5 μM ML162
1 μM ML210
5 μM Era
5 μM Fer-1
C
CFPAC1
scr
shKRAS
% Cell death
RSL3 (μM)
5 μM Fer-1
D
CFPAC1
Relative KRAS mRNA level
shScr
shKRAS
E
Response to ML162
ML162 AUC
KRASwt
KRASmut
F
Response to ML162
ML162 AUC
RASlow
RAShigh
G
Response to RSL3
RSL3 AUC
RASlow
RAShigh
H
Response to ML210
ML210 AUC
RASlow
RAShigh
I
Response to erastin
erastin AUC
RASlow
RAShigh

Figure 1

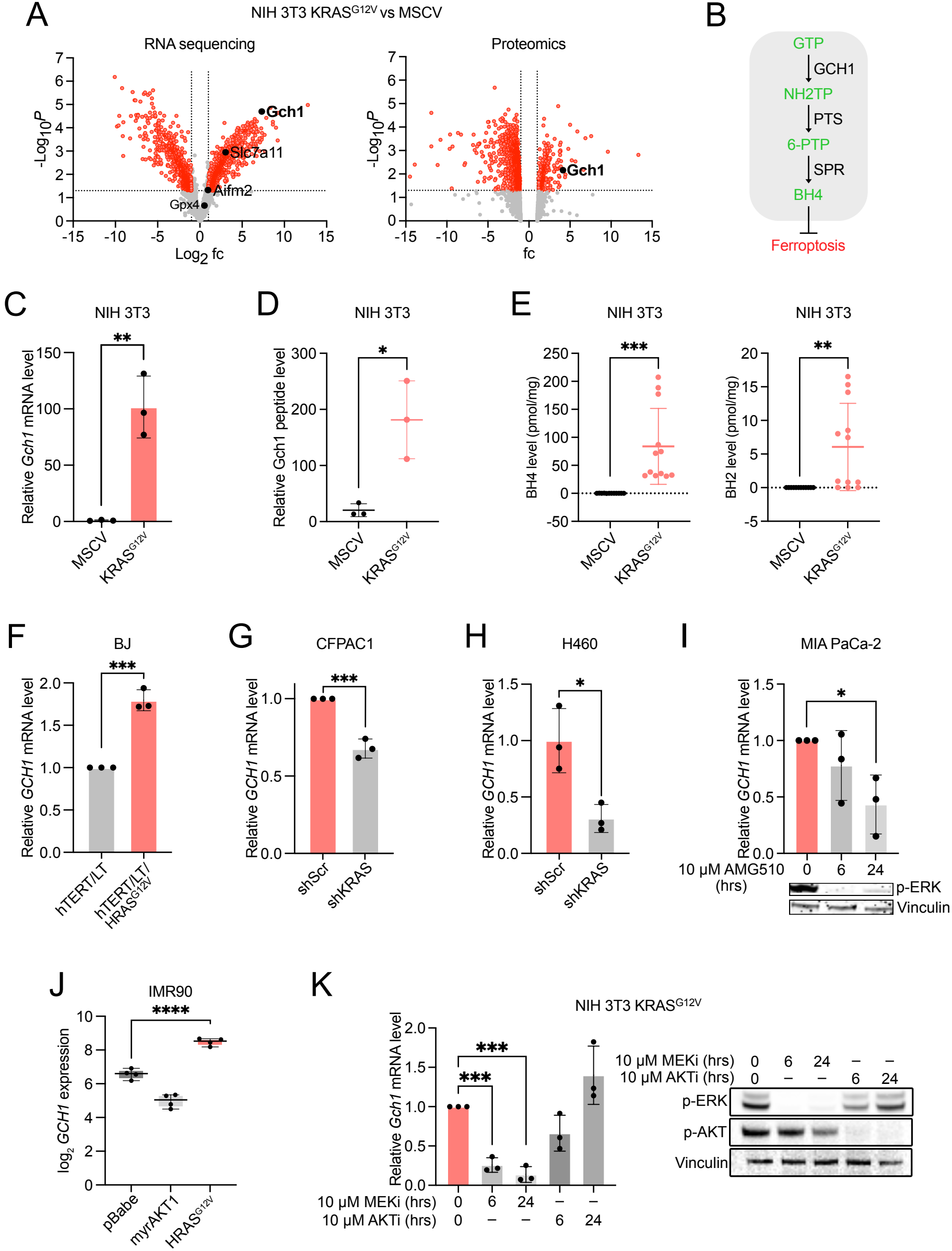
A
NIH 3T3 KRAS^{G12V} vs MSCV
RNA sequencing
Proteomics
-Log$_{10}$P
Log$_2$ fc
fc
Gch1
Slc7a11
Aifm2
Gpx4
B
GTP
GCH1
NH2TP
PTS
6-PTP
SPR
BH4
Ferroptosis
C
NIH 3T3
Relative Gch1 mRNA level
MSCV
KRAS^{G12V}
D
NIH 3T3
Relative Gch1 peptide level
E
NIH 3T3
BH4 level (pmol/mg)
NIH 3T3
BH2 level (pmol/mg)
F
BJ
Relative GCH1 mRNA level
hTERT/LT
hTERT/LT/ HRAS^{G12V}
G
CFPAC1
shScr
shKRAS
H
H460
I
MIA PaCa-2
10 μM AMG510 (hrs)
0 6 24
p-ERK
Vinculin
J
IMR90
log$_2$ GCH1 expression
pBabe
myrAKT1
HRAS^{G12V}
K
NIH 3T3 KRAS^{G12V}
10 μM MEKi (hrs) 0 6 24 – –
10 μM AKTi (hrs) 0 – – 6 24
p-ERK
p-AKT
Vinculin

Figure 2

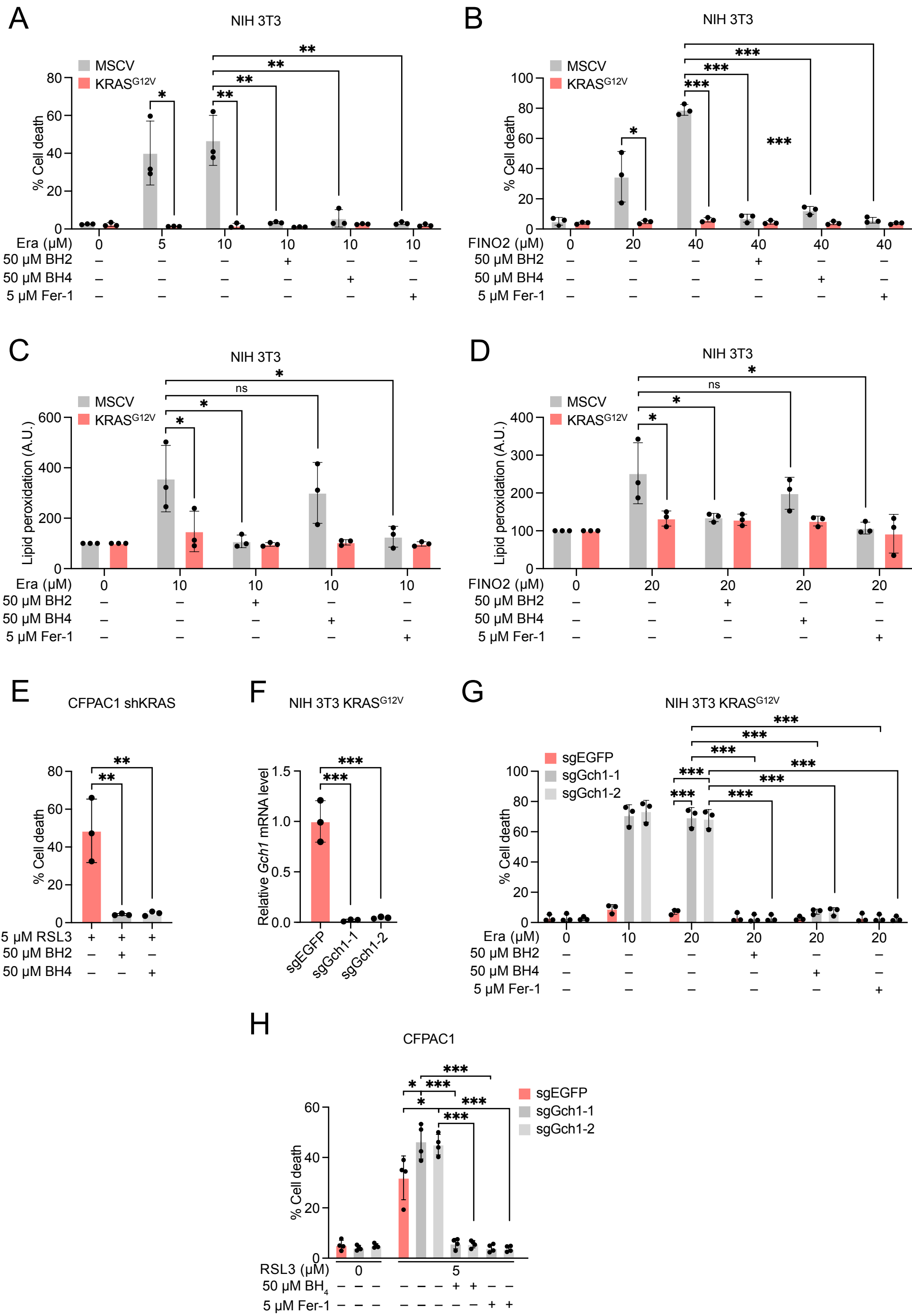
A
NIH 3T3
MSCV
KRASG12V
% Cell death
Era (μM) 0 5 10 10 10 10
50 μM BH2 – – – + – –
50 μM BH4 – – – – + –
5 μM Fer-1 – – – – – +
B
NIH 3T3
MSCV
KRASG12V
% Cell death
FINO2 (μM) 0 20 40 40 40 40
50 μM BH2 – – – + – –
50 μM BH4 – – – – + –
5 μM Fer-1 – – – – – +
C
NIH 3T3
MSCV
KRASG12V
Lipid peroxidation (A.U.)
Era (μM) 0 10 10 10 10
50 μM BH2 – – + – –
50 μM BH4 – – – + –
5 μM Fer-1 – – – – +
D
NIH 3T3
MSCV
KRASG12V
Lipid peroxidation (A.U.)
FINO2 (μM) 0 20 20 20 20
50 μM BH2 – – + – –
50 μM BH4 – – – + –
5 μM Fer-1 – – – – +
E
CFPAC1 shKRAS
% Cell death
5 μM RSL3 + + +
50 μM BH2 – + –
50 μM BH4 – – +
F
NIH 3T3 KRASG12V
Relative Gch1 mRNA level
sgEGFP
sgGch1-1
sgGch1-2
G
NIH 3T3 KRASG12V
sgEGFP
sgGch1-1
sgGch1-2
% Cell death
Era (μM) 0 10 20 20 20 20
50 μM BH2 – – – + – –
50 μM BH4 – – – – + –
5 μM Fer-1 – – – – – +
H
CFPAC1
sgEGFP
sgGch1-1
sgGch1-2
% Cell death
RSL3 (μM) 0 5
50 μM BH4 – – – – – – + + – –
5 μM Fer-1 – – – – – – – – + +

Figure 3

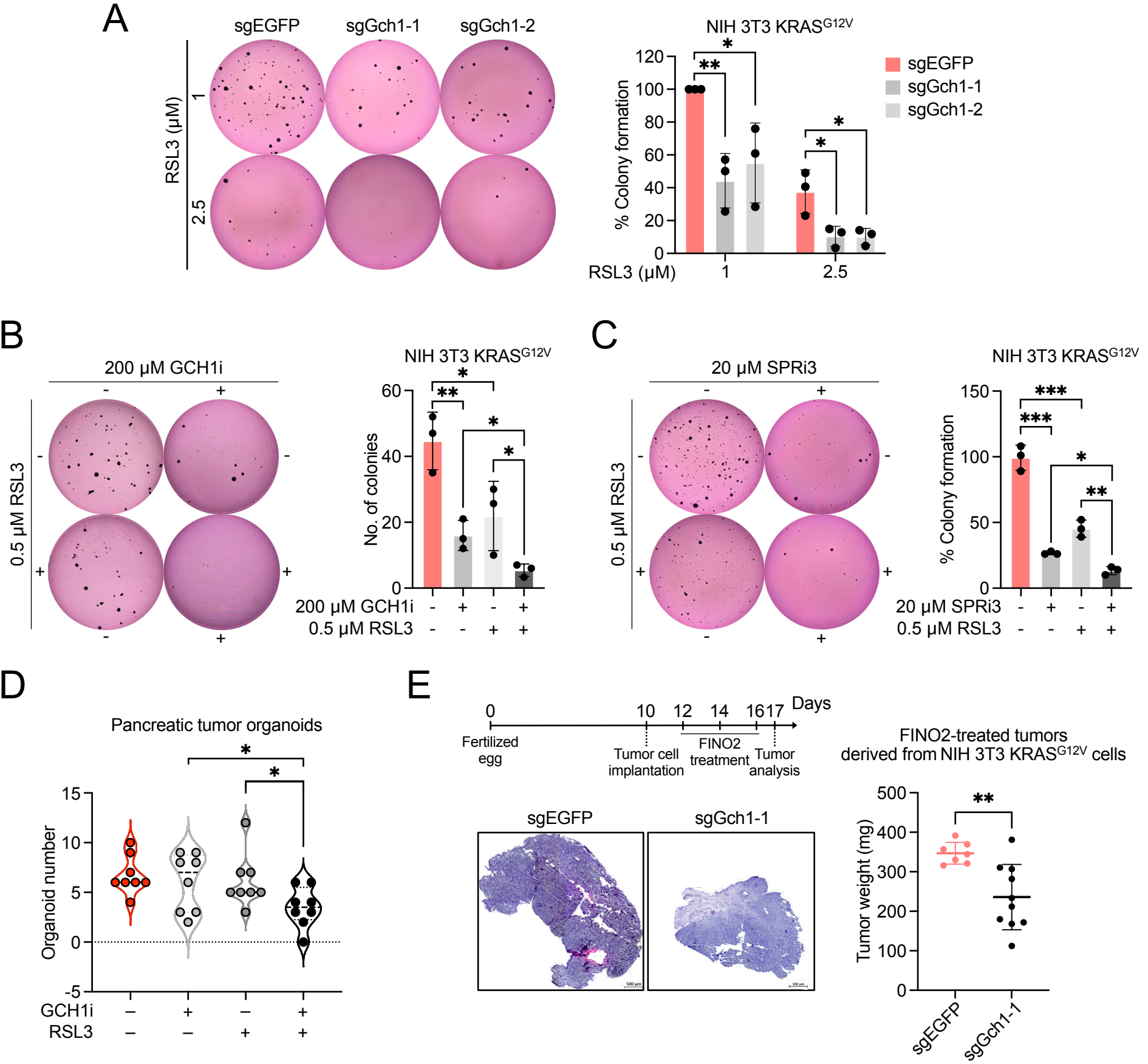
A
sgEGFP
sgGch1-1
sgGch1-2
RSL3 (μM)
1
2.5
NIH 3T3 KRAS^{G12V}
% Colony formation
sgEGFP
sgGch1-1
sgGch1-2
RSL3 (μM)
B
200 μM GCH1i
0.5 μM RSL3
NIH 3T3 KRAS^{G12V}
No. of colonies
200 μM GCH1i
0.5 μM RSL3
C
20 μM SPRi3
0.5 μM RSL3
NIH 3T3 KRAS^{G12V}
% Colony formation
20 μM SPRi3
0.5 μM RSL3
D
Pancreatic tumor organoids
Organoid number
GCH1i
RSL3
E
Days
Fertilized egg
Tumor cell implantation
FINO2 treatment
Tumor analysis
FINO2-treated tumors derived from NIH 3T3 KRAS^{G12V} cells
sgEGFP
sgGch1-1
Tumor weight (mg)
sgEGFP
sgGch1-1

Figure 4

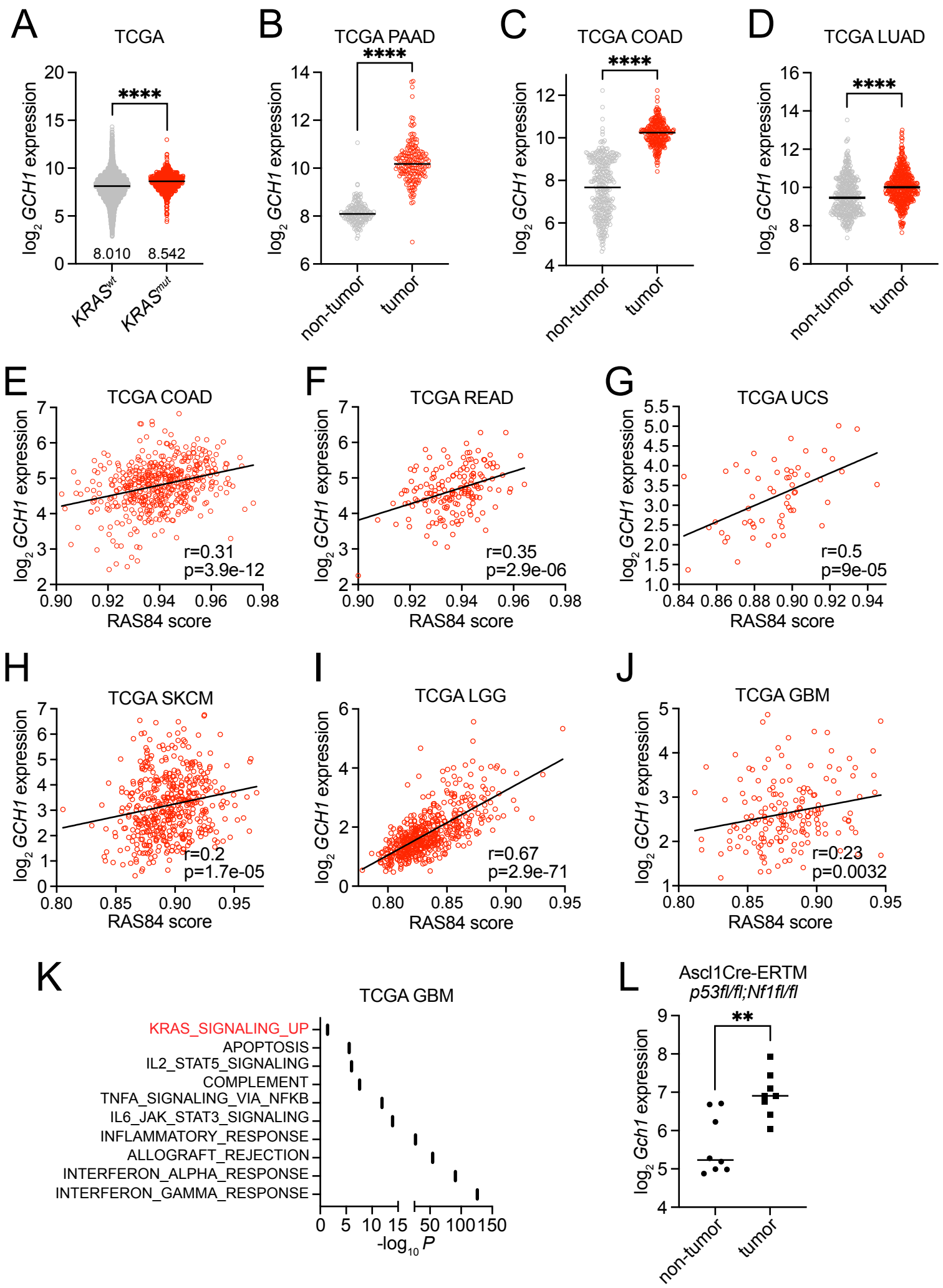
A
TCGA
****
log2 GCH1 expression
8.010
8.542
KRASwt
KRASmut
B
TCGA PAAD
****
non-tumor
tumor
C
TCGA COAD
****
D
TCGA LUAD
****
E
TCGA COAD
r=0.31
p=3.9e-12
RAS84 score
F
TCGA READ
r=0.35
p=2.9e-06
G
TCGA UCS
r=0.5
p=9e-05
H
TCGA SKCM
r=0.2
p=1.7e-05
I
TCGA LGG
r=0.67
p=2.9e-71
J
TCGA GBM
r=0.23
p=0.0032
K
TCGA GBM
KRAS_SIGNALING_UP
APOPTOSIS
IL2_STAT5_SIGNALING
COMPLEMENT
TNFA_SIGNALING_VIA_NFKB
IL6_JAK_STAT3_SIGNALING
INFLAMMATORY_RESPONSE
ALLOGRAFT_REJECTION
INTERFERON_ALPHA_RESPONSE
INTERFERON_GAMMA_RESPONSE
-log10 P
L
Ascl1Cre-ERTM
p53fl/fl;Nf1fl/fl
**
log2 Gch1 expression
non-tumor
tumor

Figure 5

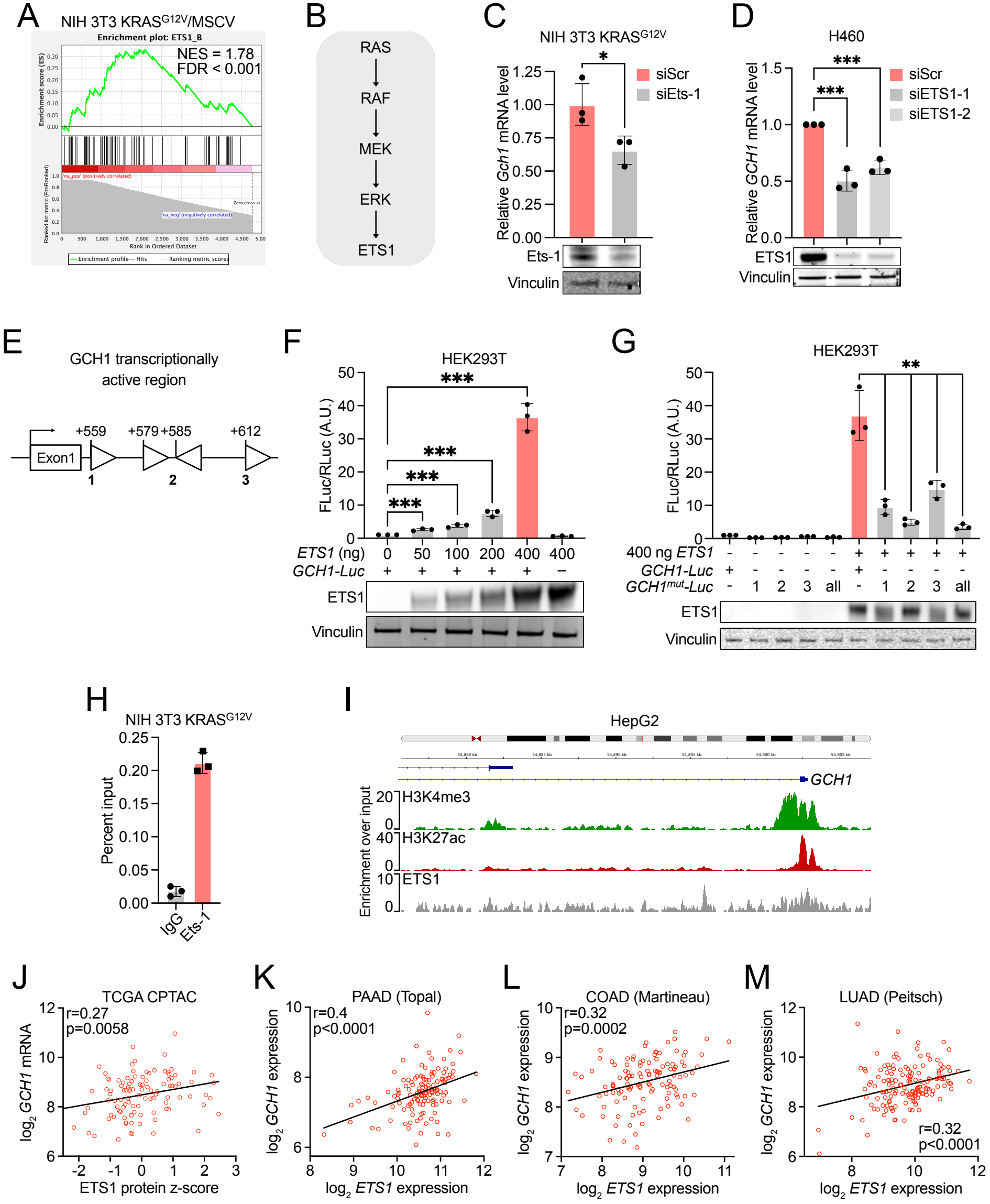
A
NIH 3T3 KRASG12V/MSCV
Enrichment plot: ETS1_B
NES = 1.78
FDR < 0.001
Enrichment score (ES)
Ranked list metric (PreRanked)
'na_pos' (positively correlated)
'na_neg' (negatively correlated)
Zero cross at
Rank in Ordered Dataset
Enrichment profile
Hits
Ranking metric scores
B
RAS
RAF
MEK
ERK
ETS1
C
NIH 3T3 KRASG12V
Relative Gch1 mRNA level
siScr
siEts-1
Ets-1
Vinculin
D
H460
Relative GCH1 mRNA level
siScr
siETS1-1
siETS1-2
ETS1
Vinculin
E
GCH1 transcriptionally active region
Exon1
+559
+579
+585
+612
1
2
3
F
HEK293T
FLuc/RLuc (A.U.)
ETS1 (ng)
GCH1-Luc
ETS1
Vinculin
G
HEK293T
FLuc/RLuc (A.U.)
400 ng ETS1
GCH1-Luc
GCH1mut-Luc
ETS1
Vinculin
H
NIH 3T3 KRASG12V
Percent input
IgG
Ets-1
I
HepG2
GCH1
H3K4me3
H3K27ac
ETS1
Enrichment over input
J
TCGA CPTAC
r=0.27
p=0.0058
log2 GCH1 mRNA
ETS1 protein z-score
K
PAAD (Topal)
r=0.4
p<0.0001
log2 GCH1 expression
log2 ETS1 expression
L
COAD (Martineau)
r=0.32
p=0.0002
log2 GCH1 expression
log2 ETS1 expression
M
LUAD (Peitsch)
r=0.32
p<0.0001
log2 GCH1 expression
log2 ETS1 expression

Figure 6

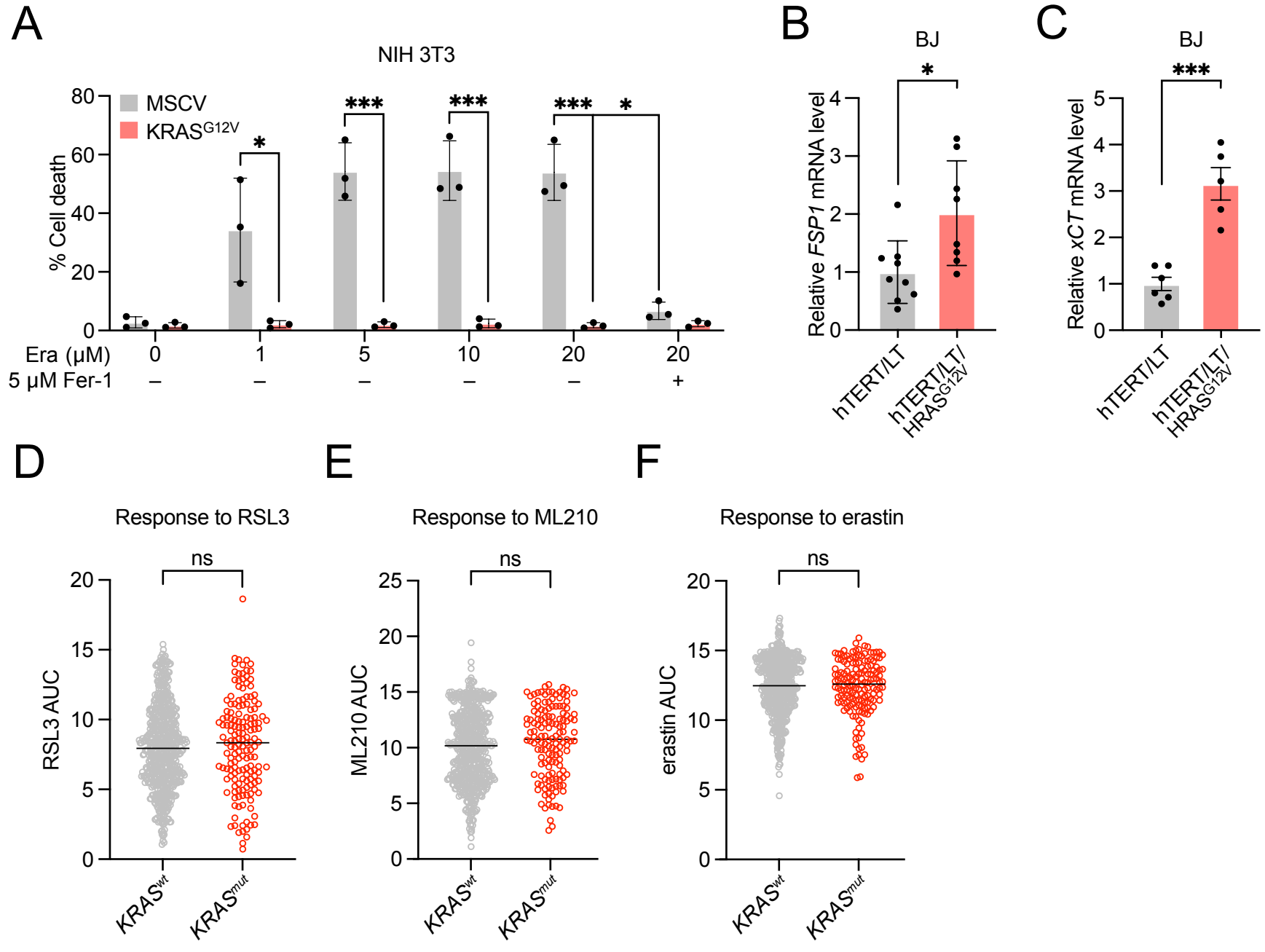

Supplementary Figure 1

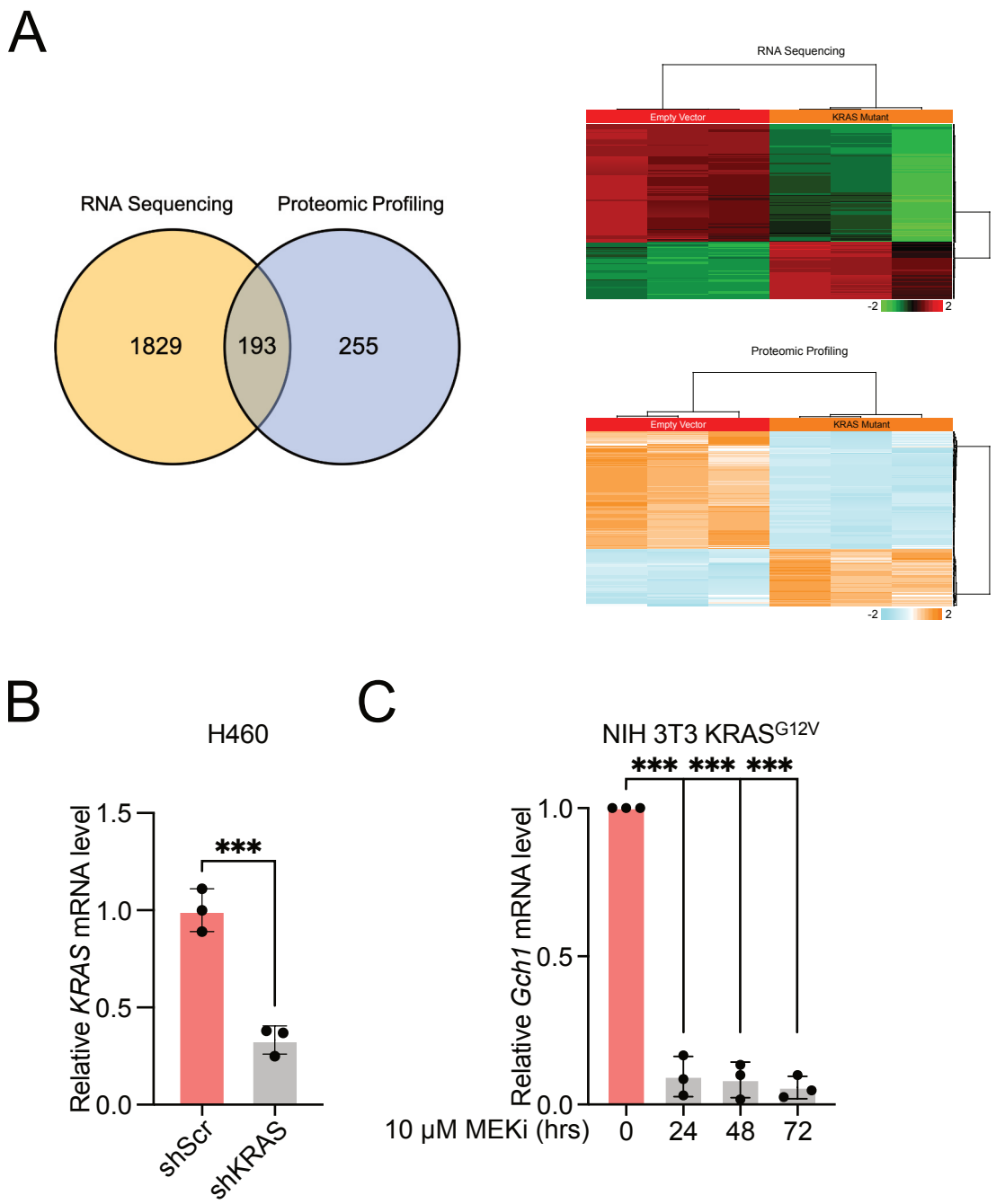

Supplementary Figure 2

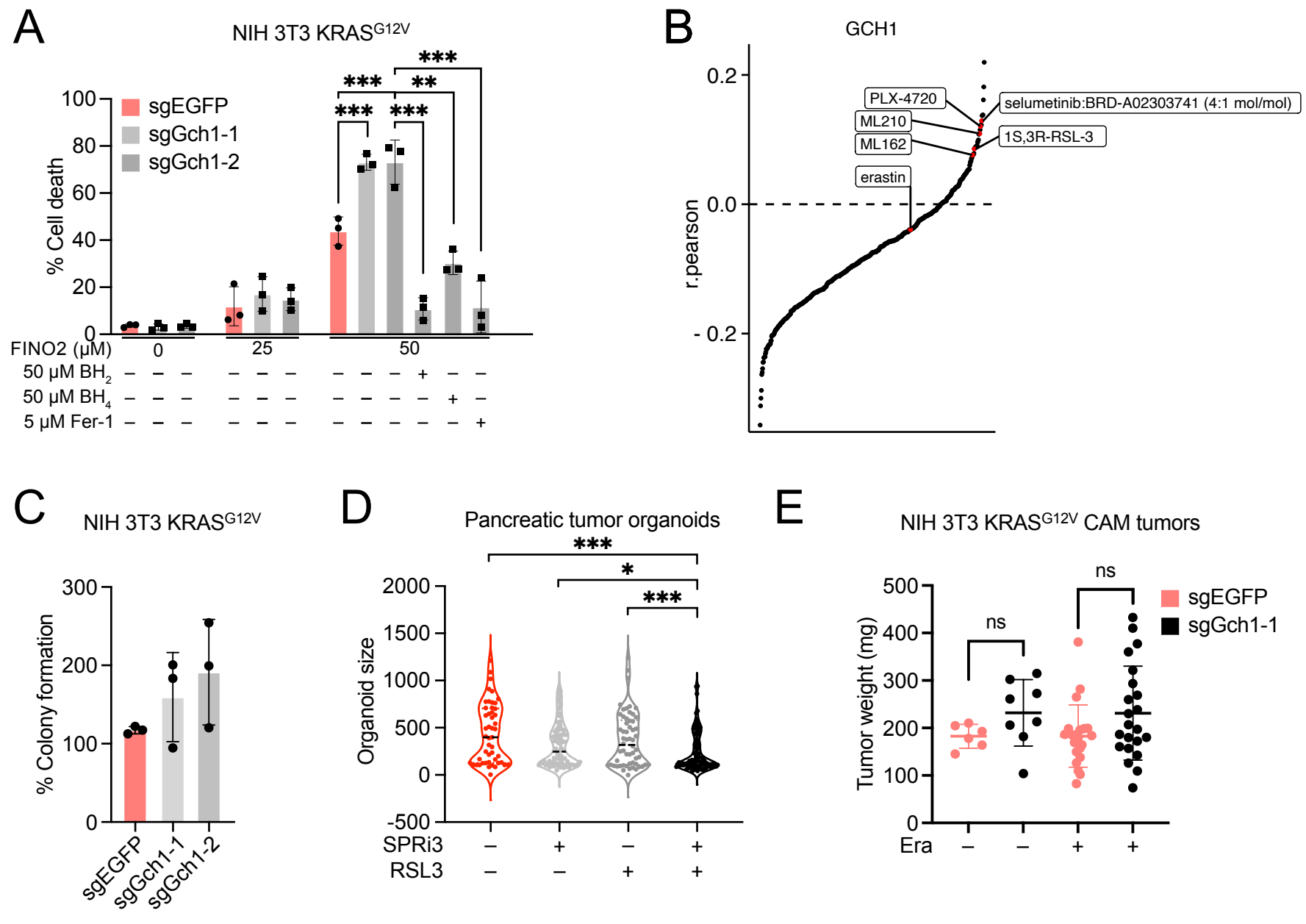

Supplementary Figure 3

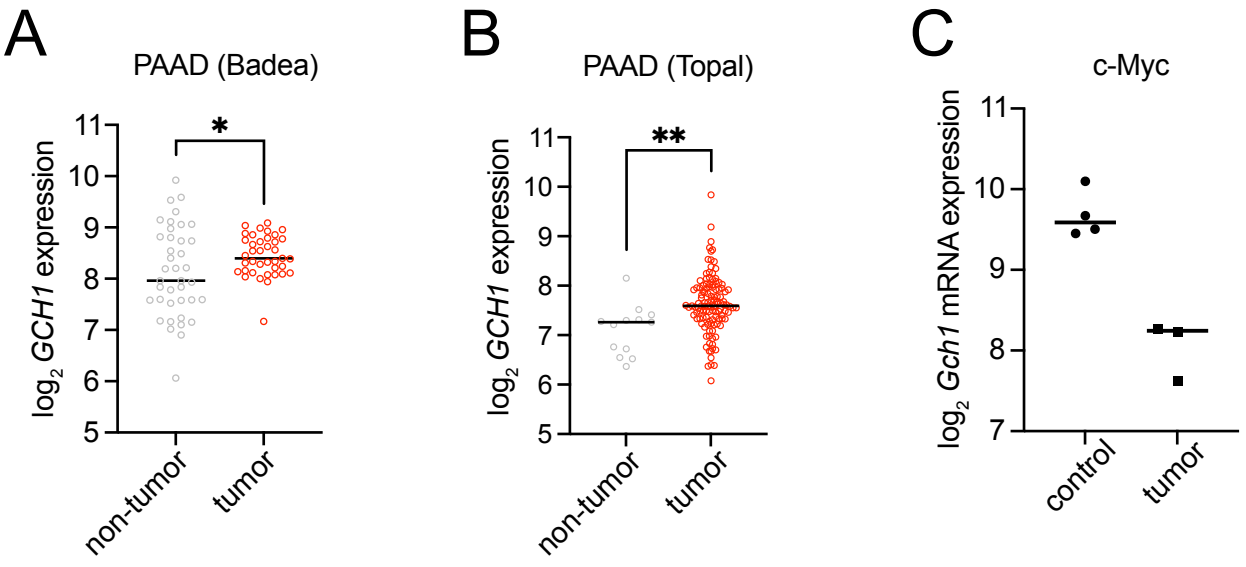

Supplementary Figure 4

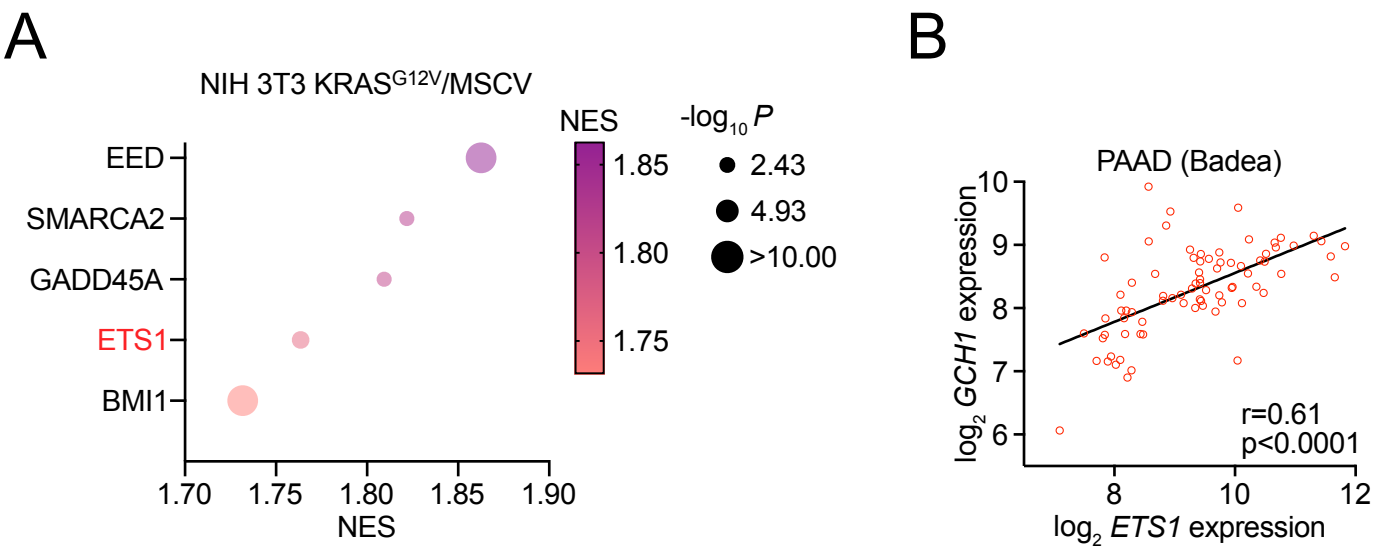

Supplementary Figure 5